

Review

Solid–Gas Thermochemical Energy Storage Materials and Reactors for Low to High-Temperature Applications: A Concise Review

Anti Kur , Jo Darkwa, John Calautit, Rabah Boukhanouf and Mark Worall

Buildings, Energy and Environment Research Group, Faculty of Engineering, University of Nottingham, Nottingham NG7 2RD, UK

* Correspondence: anti.kur@nottingham.ac.uk

Abstract: Thermochemical energy storage materials and reactors have been reviewed for a range of temperature applications. For low-temperature applications, magnesium chloride is found to be a suitable candidate at temperatures up to 100 °C, whereas calcium hydroxide is identified to be appropriate for medium-temperature storage applications, ranging from 400 °C up to 650 °C. For the high-temperature range (750–1050 °C), oxides of cobalt, manganese, and copper are found to have the redox behaviour required for thermochemical heat storage. However, some of these materials suffer from low thermal conductivities, agglomeration, and low cyclability and, therefore, require further improvements. The concept of enhancing thermal conductivities through additives such as nanomaterials has been encouraging. From an operational point of view, fluidized-bed reactors perform better than fixed- and moving-bed reactors due to better particle interactions. There is, however, a need for the reaction bed to be further developed toward achieving optimum heat and mass transfers. Agitated fluidized-bed reactors have shown encouraging results and are suggested for further exploration. A combination of appropriate computational tools can facilitate an in-depth understanding of bed dynamics.

Keywords: thermal energy storage; thermochemical energy storage; thermochemical reactors; solid–gas reactions; modelling; simulation



Citation: Kur, A.; Darkwa, J.; Calautit, J.; Boukhanouf, R.; Worall, M. Solid–Gas Thermochemical Energy Storage Materials and Reactors for Low to High-Temperature Applications: A Concise Review. *Energies* **2023**, *16*, 756. <https://doi.org/10.3390/en16020756>

Academic Editors: Alon Kuperman and Alessandro Lampasi

Received: 3 December 2022

Revised: 29 December 2022

Accepted: 4 January 2023

Published: 9 January 2023



Copyright: © 2023 by the authors. Licensee MDPI, Basel, Switzerland. This article is an open access article distributed under the terms and conditions of the Creative Commons Attribution (CC BY) license (<https://creativecommons.org/licenses/by/4.0/>).

1. Introduction

While energy supplies of various kinds and technologies underscore the economic development of societies, they also result in undesirable side effects [1]. It is common knowledge that the major environmental burden of global concern emanating from the energy sector is the greenhouse effect [2]. One of the prominent greenhouse gases (GHG) is carbon dioxide. It arises from the combustion of fossil fuels, natural gas, and coal in automobiles and power stations, as well as heating in buildings and industrial processes [2]. For instance, around 45–47% of the United Kingdom’s (UK) total energy consumption is for heating purposes, and nearly 80% is from fossil fuel sources [3]. Moreover, domestic energy use alone has a share of more than a quarter of national GHG emissions, of which 75% is for space and water heating [4]. Hence, the decarbonization of heat is the major energy challenge that the world faces over the coming decades. One way to achieve 80% emissions reduction in 2050 is by decarbonizing industrial and domestic heat demand and improving resource efficiency [2]. Current choices are around district heating (DH) networks in combination with other technologies to electrify heat or ‘green’ the gas grid [5]. However, the variability of heat demand, with a predictable winter peak heat load, presents opportunities for thermal energy storage (TES) to manage supply requirements to meet specified demands. Presently, sensible heat storage, latent heat storage, and thermochemical heat storage are the three TES systems being explored by researchers.

Sensible heat storage (SHS) is the most mature and commercially used type of TES, available as tank thermal storage for hot water and electric storage heaters [3]. This technology is utilized for its material's convective heat storage at very high temperature differences. Latent heat storage (LHS), on the other hand, is the heat absorbed or released by a substance during a change of phase. Typically, the heat is stored within a very narrow temperature range suitable only for applications requiring very small temperature differences [6]. The phase change materials (PCM) used for this purpose have the merit of achieving higher energy storage density, smaller volume requirements, and lower heat losses compared to sensible heat stores [6,7]. However, PCMs are unsuitable in comparison to SHS, which is more economical for applications requiring larger temperature differences. Thermochemical energy storage (TCES), which operates based on enthalpy change in reversible chemical reactions, is the most promising TES system [8] and has attracted greater interest in recent times.

TCES is recognized to have higher potential for energy stability and efficiency for reasons of high energy density (nearly 1000 kJ/L), smaller storage volume, minimal heat loss, long-term storage [9,10], high exergy efficiency [8], and lower charging temperature [10,11]. With respect to energy density, it is theoretically 5 to 10 times higher than LHS and SHS, respectively, when compared on the same scale basis [12,13]. As a result, the TCES system is more compact and could be effective where space constraints are significant. Additionally, TCES systems can be tuned to operate in a wide range of different temperatures and pressures [14], thus making them suitable for the storage of all grades of waste heat. This offers the possibility of being operated using various heat sources such as solar energy, aiming to operate a sustainable process. Moreover, the effective integration of TCES into district heating (DH) networks can lead to benefits such as increased energy efficiency and reliability, and reduction in energy use, costs, and GHG emissions. Thus, TCES is potentially useful in lowering fossil fuel consumption and related GHG emissions [15].

These attributes have attracted increasing interest in TCES research, albeit still at the experimental stage [3]. Many aspects of the technology are still unknown and yet to be discovered [14]. At present, TCES is hampered by a few problems, some of which include complexity in infrastructure [9] as well as low levels of thermal attainment in practical systems [9,16]. Therefore, a robust approach to operational control and understanding of the system must have a real-time model to predict its dynamics. For this reason, numerical or modelling studies are required for deeper theoretical insights and prediction of the system's behaviour. In addition, research still focuses on finding suitable materials with sufficient energy density, hydrothermal stability, and cyclability at conditions suitable for system operation [17]. Enhancement of materials' properties is crucial for integration into reactor systems. Additionally, it also requires suitable reactor optimization techniques and heat exchanger frameworks [14]. To date, experimental investigations of different reactor configurations have not overcome the dynamic limitations of heat and mass transfer [18]. In all reactors studied, nearly 70% are deployed for solid-gas reactions [19] because they show better values of chemical reaction efficiencies. However, the reaction bed must be further developed for optimum heat and mass transfers.

This paper aims to provide a concise review of the various TCES materials and reactors which could be used for low- to high-temperature applications. The review covers the fundamental concepts of TCES processes and materials, which are presented in Section 2. This includes a succinct discussion of the many experimental and theoretical efforts towards material property enhancement for application in different ranges of temperatures. The main types of solid-gas TCES reactors, together with their merits, challenges, and proposals for system improvement and optimization are discussed in Section 3. An overview of modelling and simulation of TCES systems is presented in Section 4, while the conclusion and recommendations are stated in Section 5.

We present a summary of the most recent reviews in which Desai et al. [20] reviewed sorption and chemical reactions for TCES. Experimental investigations and cyclic studies in low- and medium-temperature applications were discussed. Gbenou et al. [21] highlighted

the many research issues hampering TCES implementation. They also discussed reactor prototypes, projects, and limitations as well as suggestions for better analysis of TCES problems. Efforts to link the practical and scientific aspects of TCES problems were the focus of Sadeghi [22]. In addition, findings from cutting-edge research and pertinent aspects of the TCES system consideration were reported. Marie et al. [23] presented advances in TCES with an overview of fluidized beds for low-temperature domestic applications, whilst Kant and Pitchumani [24] focused on open and closed reactors and prototypes for building applications. A perspective on the strengths and weaknesses of TCES materials and systems as well as a discussion on the evolution of TCES research has been provided in the work of Salgado-Pizarro et al. [25]. Gbenou et al. [26] reviewed TCES reactor prototypes and projects for low-temperature applications with analyses of the microscopic and macroscopic aspects of TCES systems.

However, the above reviews covered mainly low- to medium-temperature range applications, whereas, in this review, the coverage is from low- to high-temperature applications. Reviewing the entire spectrum will help to refocus on the broader issues of TCES. This might assist in honing the possibility of combining various techniques ideal for creating composites (hybrids) with novel properties. In addition, far-reaching proposals are made for the improvement of the thermophysical properties of TCES materials as well as the performance enhancement of TCES system integration. A succinct overview of the computational tools and resources available for the modelling and simulation of TCES systems provides motivation for researchers to gain valuable insights and understanding of these systems.

2. Thermochemical Energy Storage

Generally, thermochemical energy storage (TCES) uses a reversible system in which a source provides heat, for instance, to separate reactants (AB) into products (A and B). The products are stored separately at ambient temperatures, thereby eliminating the cost of insulation in storage containers. The separation route is endothermic and is the charging process. When heat release is required, the products (A and B) are recombined and pre-heated to an activation temperature to produce the reactant (AB) through a reversible exothermic route. The reversible exothermic path is the discharging process expressed as:



where ΔH is the molar heat (enthalpy) of the reaction. Essentially, a thermochemical energy storage cycle involves three main processes [27]: (i) charging, which is the endothermic reaction requiring a heat resource to dissociate the reactant AB ; (ii) storing, where the products A and B are both stored separately; and (iii) discharging, which is the exothermic reaction where the products A and B are combined again to release heat energy.

The stored thermal energy (Q) depends on the molar reaction enthalpy (ΔH) and the number of moles (n) of one of the products [12], as in the equation:

$$Q = n\Delta H \quad (2)$$

Based on the storage mechanism, TCES processes are divided into sorption processes and reversible chemical reactions [9,13,28]. Figure 1 shows the classification chart for TCES systems. However, there appears to be a thin boundary for clear distinction between terminologies such as chemical storage, thermochemical storage, and sorption processes [27]. Often, a sorption process is considered a chemical reaction in which the chemical bonds are weak [29].

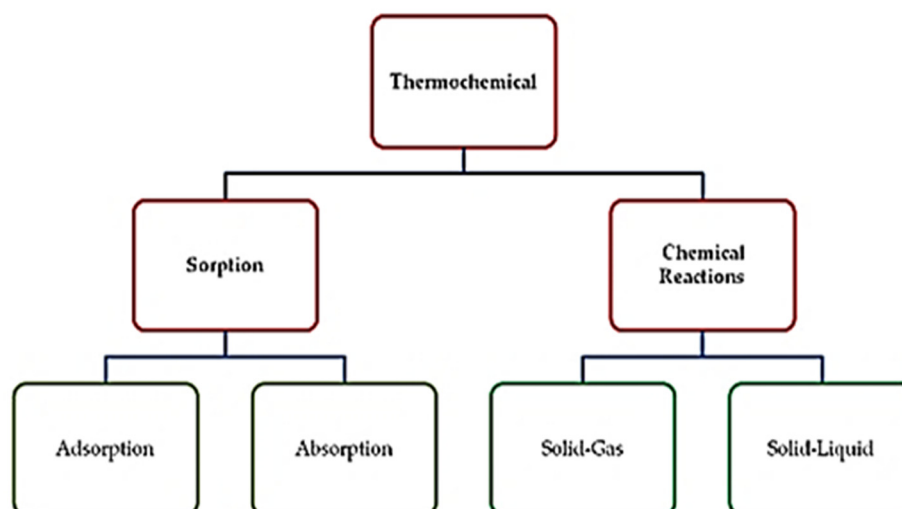


Figure 1. Classification of thermochemical energy storage systems [13].

2.1. Sorption Processes and Materials in Thermochemical Energy Storage

Sorption is described as a phenomenon by which a vapor or gas (sorbate) is captured by a denser substance (solid or liquid), called sorbent [27]. The reverse process, called desorption, requires heat to unbind the sorbate from the sorbent. Therefore, in a sorption process, heat storage is accomplished via a chemical potential when the force binding the sorbent and the sorbate is broken [30]. Essentially, absorption and adsorption are the two categories of sorption processes. Although dissimilar, they do, however, involve the physical transfer of a volume of mass or energy [27]. Absorption, in simple terms, is the process of one material (absorbent) retaining another material (absorbate). This takes place within the molecular enclave of the sorbent, resulting in alteration in its structure and morphology [17]. Examples of absorption materials for water include MgSO_4 , LiCl , LiBr , CaCl_2 , MgCl_2 , KOH , and NaOH [29].

Unlike absorption, adsorption involves a very thin layer of atoms or molecules on the adsorbent surface without altering its structure [17]. Here, there is an accumulation of energy or matter (of adsorbate) onto a surface (of adsorbent) [27]. According to Srivastava and Eames [31], adsorption is a phenomenal occurrence at the periphery of two phases where both weak intermolecular and strong chemical bonds act between the molecules. Adsorption either proceeds as a physical process, physical adsorption (physisorption), or a chemical process, chemical adsorption (chemisorption), based on the type of bond between adsorbent and adsorbate. Generally, physisorption occurs whenever an adsorbate is brought into contact with the surface of the adsorbent and involves weak intermolecular forces (Van der Waals forces) [30]. Chemisorption, on the other hand, is due to strong chemical bonds (hydrogen bonds, charge-transfer interactions, covalent bonds) [32] in the same manner as in other chemical compounds. Both types of adsorptions involve the evolution of heat. The reason that chemical forces are stronger than physical forces is that the heat of chemisorption is larger than that of physisorption [33]. Though these are different processes, they often take place simultaneously at different sites or locations of the adsorbent [30,32]. Similarly, at the mesoscale, it is difficult to distinguish between absorption and adsorption [33] as both may occur simultaneously. In that case, the term sorption is generally used for both processes [31,34].

Materials for sorption processes are usually solids, liquids, and composite sorbents with solid/gas and liquid/gas systems as working pairs [13]. Moreover, reversible adsorption of vapours onto porous solid surfaces is a potential option for TCES, particularly for space heating applications [32]. According to Yu et al. [30], the most studied adsorbents are silica gels and zeolites using water as a working fluid. In particular, zeolite 13X is the commonest and most widely studied TCES material because of its hydrothermal and mechanical stability and corrosion behaviour [13], although aluminophosphates (AlPOs),

silico-aluminophosphates (SAPOs), and metal-organic frameworks (MOFs) have recently been reviewed by Makhanya et al. [35] as promising materials for heat storage. Composite materials formed by a combination of salt hydrate and a porous additive with high thermal conductivity have also been studied [16]. Figure 2 shows a summary of typical sorption reactions and materials.

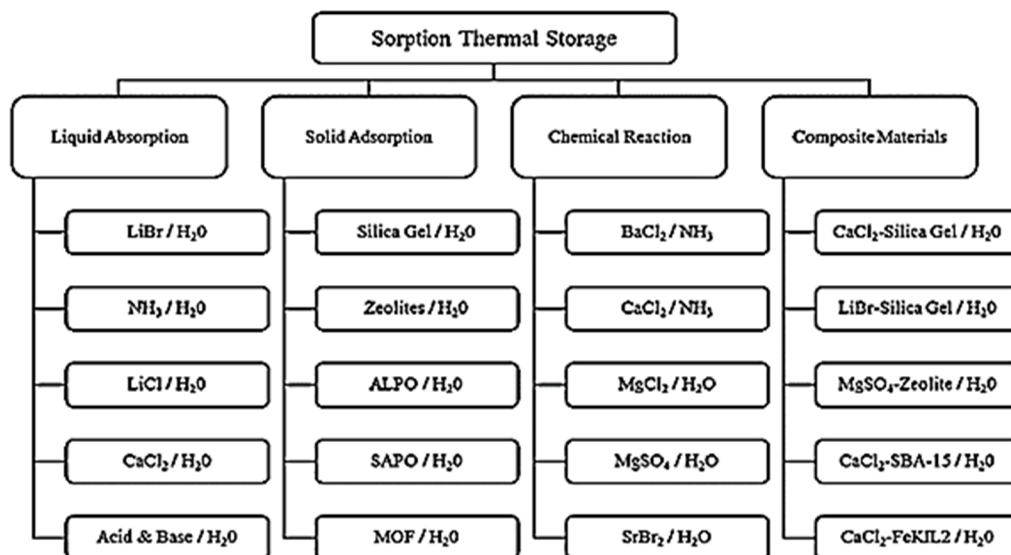


Figure 2. Sorption reactions and materials [10].

Sorption processes are essentially attractive for low-temperature applications due to their attribute of high kinetics at low temperatures [13]. Therefore, sorption reactions are typically not suitable for high-temperature applications [29].

2.2. Chemical Reactions and Materials in Thermochemical Energy Storage

TES based on chemical reactions is justifiably advantageous for seasonal storage [12]. These reaction systems store energy in the form of chemical potential, and the energy per mole required to break up chemical bonds is more than any other thermal storage system. These reactions are characterized by changes in the molecular composition of the reactants involved [13], and usually take place at temperatures above 400 °C [36]. High energy storage density and reversibility are key requirements for TCES materials, as it is challenging to find a suitable reversible reaction for a system. This is significant because the type of reaction has immense implications on the reactor design and system integration [37]. The difficult task for a reaction choice is the requirement for efficient heat and mass (HAM) transfer to and from the storage volume. This requirement, according to Aydin et al. [10] can be a limiting factor for the overall storage volume, unlike SHS and LHS, which allow higher volumes to be utilized. This volume limitation due to HAM transfer characteristics is the key area for current research in TCES systems.

In the literature [8,29,38], TCES reactions are classified into three categories, namely solid–gas, liquid–gas, and gas–gas reactions with regard to the nature of the reactants and products. However, for temperatures over 300 °C, only solid–gas and, in some cases, liquid–gas reactions remain practicable [29]. Furthermore, solid–gas reactions have been widely studied as a very promising heat storage method [39]. The interest in these reactions is due to their wide range of equilibrium temperatures and self-separation of reactants. Chemical reactions, including chemical sorption processes, premised on solid–gas systems are an encouraging method for the storage and conversion of heat energy for heating or cooling purposes [40]. While the sorption processes are used to store low (<100 °C) and medium (100–400 °C) grade heat with enthalpies in the range of 20–70 kJ/mol [40],

chemical reactions are utilized for the storage of medium (100–400 °C) and high (>400 °C) grade heat and the enthalpies are in the range 80–180 kJ/mol [13,36].

Different kinds of solid–gas reactions are employed for TCES. These are categorized depending on the composition of the solid reactant as the most prominent [38]. The reactions include those based on hydrates, hydrides, hydroxides, carbonates, and oxides. It might be important that TCES materials be flanked by an appropriate reaction temperature and enthalpy for the application. For this reason, Bauer [29] characterized the solid–gas reactions according to reaction temperatures:

- Dehydration/hydration of metal salt hydrates (in the range of 40–260 °C);
- Dehydrogenation/hydrogenation of metal hydrides (in the range of 80–400 °C);
- Dehydration/hydration of metal hydroxides (in the range of 250–600 °C);
- Decarbonation/carbonation of metal carbonates (in the range of 100–950 °C);
- Deoxygenation/oxygenation of metal oxides (in the range of 600–1000 °C).

2.2.1. Dehydration/Hydration of Metal Salt Hydrates

TCES materials for low-temperature applications have attracted remarkable attention. Salt hydrates and composite sorbents based on salt hydrates belong to this category. They have become preferred materials for TCES in building applications [41] due to their high energy density and low turning temperatures [42]. The low turning temperatures are suitable for integration with sources such as solar energy or low-grade waste heat and make them fit for residential space heating applications [42]. Much literature is available on high-potential salts, and this includes chlorides—LiCl [43], CaCl₂ [44–46], and MgCl₂ [47]; bromides—SrBr₂ [48,49] and LiBr [43,50]; and sulphates—MgSO₄ [46,47,51], Al₂(SO₄)₃ [46,52], and CuSO₄ [53]. Furthermore, other promising hydrates such as Na₂S and K₂CO₃ were studied by de Jong et al. [54] and Gaeni et al. [55], respectively.

TCES materials must fulfil common conditions such as low cost, being non-poisonous, and non-corrosive, in addition to having sufficient energy density and suitable turning temperatures. These requirements are fulfilled by many salt hydrates [46]. However, numerous salts proposed for low-grade thermal energy storage have failed [42]. In a typical case, for instance, van Essen et al. [46] conducted a theoretical study of four salt hydrates, namely MgSO₄·7H₂O, Al₂(SO₄)₃·18H₂O, CaCl₂·2H₂O, and MgCl₂·6H₂O, using a thermogravimetry and differential scanning calorimetry (TG-DSC) apparatus. Based on the measured temperature lift under practical conditions, MgCl₂ was considered the most promising with a high theoretical energy density of 2.8 GJ/m³. However, both hygroscopic chlorides under investigation tended to form a gel-like material (due to melting or formation of solution) during the hydration experiments, which prohibited further water uptake. Similarly, Donkers et al. [53] studied the cyclability of CuCl₂, CuSO₄, MgCl₂, and MgSO₄ in hydration/dehydration reactions. They observed the effect of fracturing to be greater in hydrates with larger volumetric changes. In conclusion, CuCl₂ was adjudged the most promising heat storage material.

A systematic evaluation of 125 salt hydrates was performed by N'Tsoukpoe et al. [52] using criteria such as safety, theoretical calculations, and thermogravimetry analysis (TGA). Out of 45 preselected salt hydrates, SrBr₂·6H₂O and LaCl₃·7H₂O appeared to be the most promising. However, the expected efficiency and net energy storage density (including water storage) remained low. Similarly, a review of 563 reactions was carried out [56] to evaluate the theoretical suitability of salt hydrates as seasonal heat storage materials. Up to 25 salt hydrates were identified. By considering cost, chemical stability, reaction kinetics, and safety, K₂CO₃ was determined to be the most promising candidate, but low energy density was noticed.

Table 1 gives the theoretical and experimental energy density, reaction temperature, and water vapour pressure of some salt hydrates (extracted from [57]). It is, however, noteworthy that in all these comparative investigations, the difference in behaviour is attributable to the intrinsic properties (crystal structure and thermodynamics) of the materials. Therefore, a general kinetic model of the sorption process in salt hydrates will require

specific information on the material properties. Thus, besides the high potential shown by some salt hydrates, several associated issues are still obvious. These include poor hydrothermal stability, slow thermodynamics, high corrosivity, and toxicity [41]. Such attributes make it difficult for monomer salt hydrates to be used for TCES without modification of their properties. For this reason, researchers have experimented with composite materials. Fopah Lele et al. [48] evaluated four salt hydrates (CaCl_2 , MgCl_2 , SrBr_2 , and MgSO_4) and host matrices (activated carbon, expanded natural graphite, and silica gel). The results on both systems for only salts gave thermal conductivity in the range of 0.3–1.3 W/mK with a measurement uncertainty of less than 14%. Zhao et al. [58] mixed SrBr_2 and expanded natural graphite treated with sulphuric acid. The composite with 10 wt% of SrBr_2 proved satisfactory with good mass transfer performance and no degradation in water uptake.

Table 1. Thermodynamic properties of some salt hydrates [57].

Reaction	Theoretical Energy Density (GJ/m^3)	Experimental Energy Density (GJ/m^3)	Temperature (Charging/Discharging) ($^\circ\text{C}$)	Water Vapor Pressure (mbar)
$\text{MgCl}_2 \cdot 6\text{H}_2\text{O} \rightleftharpoons \text{MgCl}_2 \cdot \text{H}_2\text{O} + 5\text{H}_2\text{O}$	2.5	0.71	150/30–50	13
$\text{MgCl}_2 \cdot 4\text{H}_2\text{O} \rightleftharpoons \text{MgCl}_2 \cdot 2\text{H}_2\text{O} + 2\text{H}_2\text{O}$	1.27	1.10	118/n.a.	13
$\text{CaCl}_2 \cdot 2\text{H}_2\text{O} \rightleftharpoons \text{CaCl}_2 + 2\text{H}_2\text{O}$	1.1	n.a.	95	n.a.
$\text{Al}_2(\text{SO}_4)_3 \cdot 6\text{H}_2\text{O} \rightleftharpoons \text{Al}_2(\text{SO}_4)_3 + 6\text{H}_2\text{O}$	1.9	n.a.	150	n.a.
$\text{MgSO}_4 \cdot 6\text{H}_2\text{O} \rightleftharpoons \text{MgSO}_4 \cdot \text{H}_2\text{O} + 5\text{H}_2\text{O}$	2.37	1.83	72/n.a.	13
$\text{MgSO}_4 \cdot 7\text{H}_2\text{O} \rightleftharpoons \text{MgSO}_4 \cdot \text{H}_2\text{O} + 6\text{H}_2\text{O}$	2.3	n.a.	150/105	n.a.
$\text{CaSO}_4 \cdot 2\text{H}_2\text{O} \rightleftharpoons \text{CaSO}_4 + 2\text{H}_2\text{O}$	1.4	n.a.	n.a./89	n.a.
$\text{Na}_2\text{S} \cdot 5\text{H}_2\text{O} \rightleftharpoons \text{Na}_2\text{S} \cdot 1/2\text{H}_2\text{O} + 9/2\text{H}_2\text{O}$	2.7	n.a.	80/65	13
$\text{SrBr}_2 \cdot 6\text{H}_2\text{O} \rightleftharpoons \text{SrBr}_2 \cdot \text{H}_2\text{O} + 5\text{H}_2\text{O}$	2.3	2.08	n.a./23.5	20
$\text{Li}_2\text{SO}_4 \cdot \text{H}_2\text{O} \rightleftharpoons \text{Li}_2\text{SO}_4 + \text{H}_2\text{O}$	0.92	0.80	103/n.a.	13
$\text{CuSO}_4 \cdot 5\text{H}_2\text{O} \rightleftharpoons \text{CuSO}_4 \cdot \text{H}_2\text{O} + 4\text{H}_2\text{O}$	2.07	1.85	92/n.a.	13

n.a.: not available.

Salt mixtures appear promising, but the general technical issue reported is mass transport within the matrix's pores due to deliquescence, overhydration (with possible leakage or pore blockage), and a low-temperature lift [41]. A proposal for pairing suitable salt hydrates according to different matrix materials, reactor analyses, and structural optimization methods for the enhancement of HAM transfer has recently been published [59]. Again, selecting a suitable binary salt mixture may increase the performance of each material and avoid its unique individual shortcomings. A double salt hydrate, $\text{Na}_2\text{Zn}(\text{SO}_4)_2 \cdot 4\text{H}_2\text{O}$, has been reported as having exhibited suitable stability at the first ten hydration/dehydration cycles, with an excellent energy storage density of 4.7 GJ/m^3 and theoretical efficiency up to 77.4% [60]. It might be necessary that the influence of material characterization and reaction parameters are considered to determine the optimum mixing pair and ratio, as well as optimize system controls under different operating conditions [41]. In spite of this, N'Tsoukpoe and Kuznik [34] assert that the performance achieved with salt-hydrate systems is not competitive and that the performance or advantages of the TCES materials have probably been overestimated.

2.2.2. Dehydrogenation/Hydrogenation of Metal Hydride

Metal hydrides (MHs) are compounds formed by the reversible reaction of hydrogen and metal or metal alloy, and this reversible absorption of hydrogen gas is exothermic [39]. The utilization of MHs for TCES is encouraged due to high energy efficiency, high volumetric energy density, and cost [61]. It also offers flexibility in its wide range of operating temperatures. On the other hand, one of the main disadvantages of MH systems is the need for hydrogen storage [37]. This means that the MH system can be a closed system with an intermediate hydrogen storage subsystem. It is suggested that by coupling a high temperature with a low-temperature metal hydride system, a self-regulating reversible metal hydride energy storage system can be established [62].

Lithium hydride (LiH), calcium hydride (CaH₂), and magnesium hydride (MgH₂) systems have been studied for their TCES potentials. However, more attention has been paid to MgH₂ [9]. It has a working temperature between 200–500 °C and decomposes into Mg metal, releasing hydrogen with a reaction enthalpy of 75 kJ/mol and a heat storage capacity of around 0.8 kWh/kg [39,63]. The hydrogen gas can be stored in a reservoir under the equilibrium pressure of MgH₂. For instance, the MgH₂/Mg equilibrium pressure of 10 bar at 350 °C and 20 bar at 400 °C is shown in Figure 3. According to Felderhoff et al. [39], if the pressure is lower than the equilibrium pressure at a given temperature (coloured area in Figure 3), MgH₂ decomposes until the pressure inside the system reaches the equilibrium pressure. At pressures higher than the equilibrium pressure, Mg metal can be hydrogenated (white area in Figure 3).

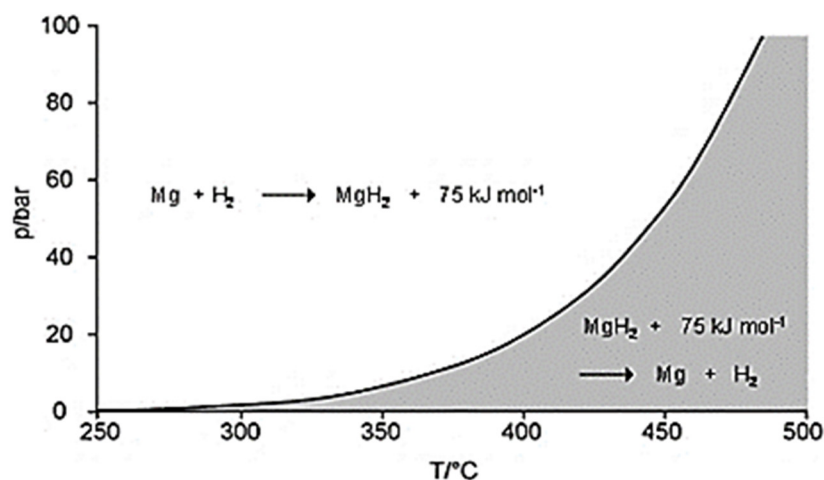


Figure 3. Equilibrium pressure of MgH₂ as a function of temperature [39].

Chen et al. [9] noted that the MgH₂/Mg pair suffers from poor reversibility. Its cyclic stability drops by 75% after 500 cycles [8] which is a limiting factor in large-scale application. Additionally, its high thermodynamic stability and sluggish sorption kinetics are the major obstacles to its extensive application [64]. Table 2 shows the thermodynamic properties of MgH₂ [65].

Table 2. Thermodynamic parameters and energy storage properties of MgH₂ [65].

Thermodynamic Parameters	Values
Formation enthalpy, kJ/(mol.H ₂)	−74.5
Formation entropy, J/(mol.H ₂ .K)	−135
Hydrogen Storage Capacity (Theoretical)	
Gravimetric capacity, wt%	7.6
Volumetric capacity, g/(L.H ₂)	110
Thermal Energy Storage Capacity (Theoretical)	
Gravimetric capacity, kJ/kg	2204
Volumetric capacity, kJ/dm ³	1763

Strategies employed to overcome these issues include the addition of nanostructures, alloying, and MgH₂-based composites. The catalytic addition of different transition metals or transition metal oxides can greatly accelerate the hydrogenation/dehydrogenation kinetics [39]. Khan et al. [66] investigated two nanostructured MgH₂ and cobalt (Co) powders. The hydrogen storage properties of the 2MgH₂-Co powder and 2MgH₂-Co compressed pellet were analysed. Fast hydrogenation was observed in the de-hydride 2MgH₂-Co compressed pellet, with about 2.75 wt% absorbed in less than 1 min at 300 °C, and a maximum hydrogen storage capacity of 4.43 wt%. The hydrogen absorption activation energy of the 2MgH₂-Co compressed pellet was also lower than in the 2MgH₂-Co

powder. Banrejee et al. [67] prepared nanocrystalline magnesium and compared it with micro-crystalline magnesium. The developed nanocrystalline Mg exhibited improved properties with a higher hydrogen storage capacity of 6.24 wt% at 300 °C. Prolonged ball milling led to faster hydrogenation kinetics (up to 90% of the saturation value in 15.5 min at 250 °C) and a substantial decrease in the activation barrier. Nanostructuring has also been studied [68,69] with remarkable improvements in Mg-based storage properties. However, nanostructuring could result in poor thermal conductivity [9]. Additionally, the drawback in powder materials is usually due to their tendency towards coarsening and sintering during dehydrogenation/hydrogenation cycles. This is susceptible in Mg, which has a relatively low melting temperature and, thus, displays significant atomic mobility at the cycle operating temperatures [66].

Alloying is an effective and easy-to-handle method of improving the sorption property of MgH₂/Mg [9]. Intermetallic compounds of transition metals are among the catalytic materials that can facilitate the thermal storage processes in MgH₂ [69]. Usually, intermetallic hydrides are composites of a hydride-forming element at high temperatures and a non-hydride-forming element, such as Mg₂NiH₄ and Mg₂FeH₆. Research efforts aimed at reducing the reaction temperatures of these composite hydrides have been achieved through the addition or substitution of existing elements [70]. There seems to be a consensus that increasing the number of 3D elements would improve the kinetics by decreasing the activation energy of hydrogen desorption [71]. For instance, the enthalpy change associated with the formation of Mg₂FeH₆ at 500 °C was measured to be 77.4 kJ/mol H₂, lower than the reported values of 98 kJ/mol H₂ [62]. Zhang et al. [64] also reported a decrease in the hydrogen desorption enthalpy and initial dehydrogenation temperature of MgH₂ through incorporation of either Ti or Ni. Sulaiman et al. [72] reported that a 5 wt% K₂NiF₆-doped MgH₂ sample started desorbing around 260 °C, which was a reduction of about 95 °C and 157 °C compared with the as-milled and as-received MgH₂. Additionally, the de/absorption kinetics were also improved significantly compared to the un-doped MgH₂. In another approach, Majid et al. [73] selected TiFe_{0.8}Mn_{0.2}, graphite, and Fe as additives. Compared to pure milled MgH₂ powder, they found that the dehydrogenation peak temperatures were decreased by 90, 160, and 165 °C for Mg-TiFe_{0.8}Mn_{0.2}-graphite, Mg-Fe-graphite, and Mg-TiFe_{0.8}Mn_{0.2}-Fe-graphite composites, respectively. The co-addition of TiFe_{0.8}Mn_{0.2}, graphite, and Fe exhibited synergistic effects in improving the hydrogen desorption properties of MgH₂.

The roles of Ti-based catalysis and its consequent hydrogen storage effects on MgH₂ were reviewed by Zhou et al. [65]. They concluded that the doping technique via Ti-based catalysis is a viable approach to enhancing the reaction of Mg-based materials. A comprehensive compilation of Ti-based catalysis of MgH₂ systems, corresponding synthesis approaches, and kinetic behaviours is presented in their review. On the other hand, Kumar et al. [74] performed calculations based on the first principles to investigate the dehydrogenation kinetics, considering doping at various layers of MgH₂ (110) surface with Ca, Al, Ga, Sc, Ni, Ti, and V. Doping at the first and second layers of MgH₂ (110) had a significant role in lowering the H₂ desorption (from surface) barrier energy. The screening approach found Al and Sc to be the best possible dopants at lowering desorption temperature while preserving similar gravimetric density and bulk modulus to a pure MgH₂ system. By extending frontiers, Jain et al. [75] conducted an investigation on the role of alkaline metal fluoride (MgF₂) as a catalyst in the hydrogen-storage behaviour of MgH₂. For 5 mol% MgF₂ admixed into MgH₂ powder, hydrogenation measurements at 335 °C showed 92% of absorbed theoretical capacity in less than 20 min (compared to 70% by pure MgH₂). Sorption studies further point to the possibility of complete absorption at low temperatures down to 145 °C. Again, cyclic measurements made at 310 °C revealed an inconsequential loss in the total storage capacity. These results implied that the sensitivity of the material to atmospheric conditions is low, and it is easy to handle. Thus, it can be employed in applications where operation at relatively high temperatures is insignificant.

A variety of dopants for MgH_2 has been reported and the respective Mg-based hydride materials have been enhanced. Despite improvement in the material properties, thermodynamic tuning remains a major challenge [76]. Present approaches have been successful in addressing it, to some extent, but much is still desired for practical application.

2.2.3. Dehydration/Hydration of Metal Hydroxides

Thermochemical heat storage with metal hydroxides results from a reversible reaction of water (steam) and metal oxides at high temperatures (~ 500 °C) and near-atmospheric pressures [8]. The alkaline earth metal hydroxides such as $\text{Mg}(\text{OH})_2$, $\text{Ca}(\text{OH})_2$, $\text{Sr}(\text{OH})_2$, or $\text{Ba}(\text{OH})_2$ have been considered as storage materials [39]. The initial candidate hydroxide–oxide pairs are $\text{Mg}(\text{OH})_2/\text{MgO}$, $\text{Ca}(\text{OH})_2/\text{CaO}$, $\text{Sr}(\text{OH})_2/\text{SrO}$, and $\text{Ba}(\text{OH})_2/\text{BaO}$. The theoretical turning temperatures and thermodynamic data of these hydroxides are presented in Table 3. The reactions are in the range of 70–1005 °C, though most of the reactions are too low for high-temperature application [11], usually occurring at medium temperatures of $250 < T < 450$ °C. The steam partial pressure and the temperature drive the hydration/dehydration reactions [12]. Figure 4 shows some of the couples which could be used for TCES application.

Table 3. Equilibrium temperature and heat storage capacity of metal hydroxides [11].

Material	Temperature (°C)	Reaction Enthalpy (kJ/mol)	Gravimetric Energy Density (kJ/kg)
$\text{Ca}(\text{OH})_2/\text{CaO}$	515	100.177	1352
$\text{Mg}(\text{OH})_2/\text{MgO}$	265	77.745	1333
$\text{Be}(\text{OH})_2/\text{BeO}$	70	51.276	1191
$\text{Mn}(\text{OH})_2/\text{MnO}$	190	67.072	754
$\text{Sr}(\text{OH})_2/\text{SrO}$	755	88.581	728.3
$\text{Ba}(\text{OH})_2/\text{BaO}$	1005	93.462	545.47
$\text{Ni}(\text{OH})_2/\text{NiO}$	70	47.846	516
$\text{Zn}(\text{OH})_2/\text{ZnO}$	55	49.609	498.96
$\text{Cd}(\text{OH})_2/\text{CdO}$	125	59.952	409.4

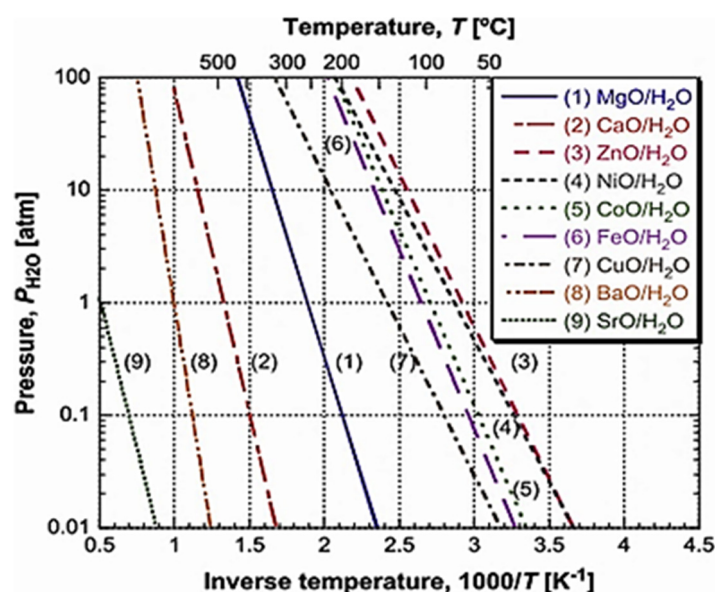


Figure 4. Reaction equilibrium lines for metal oxide/water reaction systems [8].

With reference to the high reaction enthalpies and energy storage densities (Table 3), mainly the hydroxides $\text{Ca}(\text{OH})_2$ and $\text{Mg}(\text{OH})_2$ have been extensively studied theoretically and experimentally [9,39]. However, the $\text{Ca}(\text{OH})_2/\text{CaO}$ system is more attractive [10]. It is

the most-explored hydroxide system for thermochemical energy storage, prompting tests in both lab-scale reactors and TGA [14]. One reason is that the hydration of MgO is very slow in superheated steam and the rate of reaction drops with the rise in temperature [8,39]. Figure 5 shows the decomposition of the Mg(OH)₂ system at a relatively low temperature of around 330 °C [9]. The reaction enthalpy of Mg(OH)₂ degenerates with temperature up to 500 °C, unlike the enthalpy of Ca(OH)₂. In addition, CaO has a higher heat of adsorption over a short period [77] than MgO, as well as being much cheaper [8]. In view of these attractive attributes, a plethora of research efforts has been conducted for the potential application of Ca(OH)₂/CaO as a long-term thermal energy storage system.

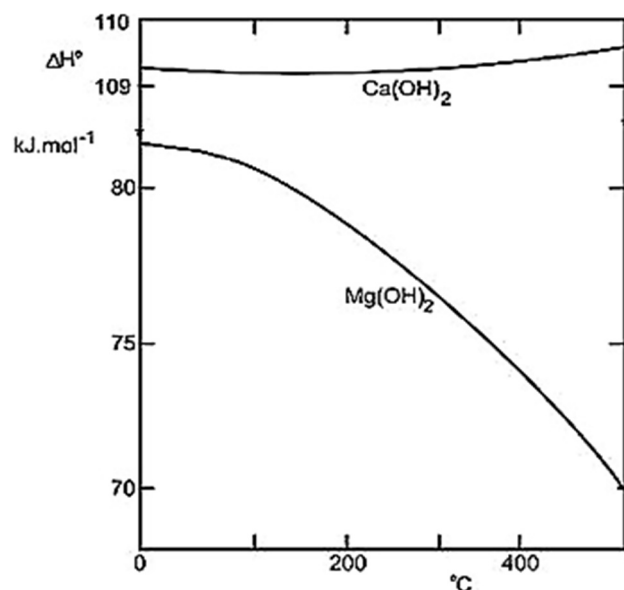


Figure 5. Enthalpy of dehydration reaction is dependent on temperature for Ca(OH)₂ and Mg(OH)₂ [39].

Schaube et al. [78] investigated a 10 mg sample in a Ca(OH)₂/CaO reversible system, and full conversion and cycling stability were reported over 100 cycles at a water partial pressure of 1 bar (even at 0.956 bar), with an equilibrium temperature of 505 °C and enthalpy of 104.4 kJ/mol. However, little success was achieved in the cycling stability of a 60 g sample of the reaction system as degradation was reported over 25 cycles. Agglomeration was also observed [79]. Additionally, Criado et al. [80] investigated Ca(OH)₂/CaO hydration/dehydration reaction and obtained higher rates than those reported in the literature at temperatures in the range of 400–560 °C and partial steam pressures between 0 and 100 kPa. However, particle attrition was observed for large particle sizes of the material. In another work, Dai et al. [81] investigated the cycling stability of the Ca(OH)₂/CaO system for 20 successive dehydration/hydration cycles. Existing problems relating to agglomeration, sintering, poor thermal conductivity, and irregularity in the rate of heat release were raised. There is a consensus that major problems encountered in Ca(OH)₂ reactors relate to particle agglomeration and sintering, poor heat transfer characteristics, and low permeability of the packed bed. Though the issue of permeability has been addressed in optimized reactors, other problems still exist [39]. As a result, much of the research has been around material enhancement through additives or composites, as well as reactor optimizations.

Criado et al. [82] synthesized composite materials using sodium silicate (Na₂Si₃O₇) to bind Ca(OH)₂/CaO particles for fluidized/fixed-bed application. The mechanical properties of the resulting CaO/Ca-silicate composites over hundreds of hydration/dehydration cycles were investigated. The results confirmed the primary role of Ca(OH)₂ anisotropic expansion as the main cause of the reduction in the crushing strength of the pellets. Another study by Funayama et al. [83] relates to a composite material using SiC/Si foam. The per-

formance of the ~63 g of composite material with a packed-bed reactor was evaluated. The rate of heat output per volume under maximum hydration pressure of the composite was 1.3 kW/L-bed for the first 5 min, which is 1.4 times higher than previously reported for a bed of $\text{Ca}(\text{OH})_2$ pellets. The composite material with pore size 400 μm of the $\text{CaO}/\text{Ca}(\text{OH})_2$ samples maintained high reactivity and bulk volume during cycle reactions. This study was extended by using a ceramic honeycomb support composed of SiC/Si [84]. A volumetric energy density of 0.76 MJ/L-bed was obtained, and a heat output rate 1.8 times higher than the previously reported value for the pure $\text{Ca}(\text{OH})_2$ pellet bed was achieved. In addition, the material also sustained high reactivity during the reaction cycles. Mixtures of expanded graphite (EG) with $\text{Ca}(\text{OH})_2$ were also investigated by Kariya et al. [85] with the aim of enhancing the heat transfer and reactivity of the hydroxide. The results indicated that the maximum mean heat output of a sample mixture containing 11 wt% EG was twice as high as the heat of pure $\text{Ca}(\text{OH})_2$. The decreasing effect of EG in the hydration reaction in the repetitive cycles was due to particle pulverization.

The doping of $\text{Ca}(\text{OH})_2$ by hexagonal boron nitride (HBN) was approached by Huang et al. [86]. Analysis showed improvement in both thermal conductivity and dehydration enthalpy of the material. It also revealed a 15 wt% as optimal mass content of HBN-doped composite with improved activity after 10 dehydration/rehydration cycles. In addition, a 67% rehydration conversion and energy density greater than 1000 kJ/kg were achieved. Doping of $\text{Ca}(\text{OH})_2$ with potassium nitrate, KNO_3 , has also been reported by Shkatulov et al. [87]. With a 5 wt% KNO_3 addition to $\text{Ca}(\text{OH})_2$, the dehydration temperature of the material was reduced and the reaction rates increased, but the material lost its dehydration heat by 7%. Wang et al. [88] obtained a similar result with a 10 wt% KNO_3 addition and the doped $\text{Ca}(\text{OH})_2$ further showed good cycling stability in the nitrogen atmosphere, but failed in air. Gollsch et al. [89] modified $\text{Ca}(\text{OH})_2$ powder with nanostructured flow agents to improve the powder's flowability. The additives consisted of nanostructured Si and/or Al_2O_3 . Additives of weight fractions 6–12% improved the flowability of the powder. However, after cycling, the flowability of the mixtures decreased, while that of the pure powder increased. Analysis showed a correlation between growth in particle size and increased flowability. Additionally, the formation of phases in the additives led to a decrease in absolute heat release of up to 50%, although some of the side products seemingly added to the measured heat release by hydrating exothermally.

In tackling the problem of low conductivity and cohesive nature of powder bulk material, Mejia et al. [90] investigated ceramic-encapsulated CaO granules and $\text{Ca}(\text{OH})_2$ granules coated with Al_2O_3 nanostructured particles. The results showed that both encapsulated materials did not change their shape after six-fold cycling. However, the Al_2O_3 -coated sample exhibited volume expansion during hydration. There was a reduction in the reaction activity of the ceramic sample, whereas the performance of the Al_2O_3 sample was almost the same as the unmodified $\text{Ca}(\text{OH})_2$ particles. Afflerbach et al. [91] investigated an encapsulated sample and good mechanical stability of the material was attained, followed by a considerably improved thermal conductivity. Again, over ten reaction cycles were attained in a lab-scale reactor. Additionally, issues concerning the poor flowability of the storage material and poor heat and mass transport with a strong agglomeration tendency could be overcome by persistent particle size stabilization. Of course, much is still required in terms of material enhancement, but research efforts so far show the $\text{Ca}(\text{OH})_2/\text{CaO}$ system to have higher prospects for long-term TCES application.

2.2.4. Decarbonation/Carbonation of Metal Carbonates

Decarbonation/carbonation reactions of metal carbonates have also proven to be attractive high-temperature heat storage systems. In this case, heat is used to perform the endothermic breakdown of carbonate, and the products are CO_2 and metal oxide. The interest in carbonates is due to their relatively high operating temperatures (typically over 800 °C), high volumetric density, low operating pressure, non-toxicity, abundance, and cheapness [8,13]. The decomposition of CaCO_3 , SrCO_3 , BaCO_3 , MgCO_3 , and PbCO_3 has

been studied [14]. Alas, the controversy about the high refractoriness of MgCO_3/MgO and the toxicity of PbCO_3/PbO [9] is a drawback for further research in these materials. Additionally, the carbonation reaction of BaO into BaCO_3 was hindered by the melting of the material during the decomposition step [92]. Therefore, among the carbonates, CaCO_3 is considered the most promising heat storage material [9,39] and the focus will be on the CaCO_3/CaO system. It has been reported that after 40 high-temperature carbonation/decarbonation cycles with CaO , the carbonation (adsorptive) reaction significantly decreased because of the decrease in pore volume in the material [9]. This loss in porosity is caused by a decrease in the surface area of CaO due to the sintering of the particles [14,39], thereby inhibiting CO_2 access to the active sites within the material. Several techniques have been developed to minimize this loss in adsorption capacity. To increase the active surface area and stability of the pore structure, the use of additives, reduction in the particle size, and the synthesis of novel materials with the microporous structure were proposed [93].

To this end, Lu and Wu [94] doped nano CaO with Li_2SO_4 and showed that the Li_2SO_4 -nano CaO adsorbent maintained a 51% conversion after 11 cycles, compared to pure nano CaO maintaining 27.3% under the same conditions. The superior performance of the Li_2SO_4 -nano CaO adsorbent was attributed to pore enlargement and increase in macro-pore proportion through the Li_2SO_4 addition. Moreover, there were increased reaction rates and a lowering of the decomposition temperature by 15°C in comparison with the pure material. In another work [95], different MgO concentrations were added to the CaO material. The additions with 5 and 10 wt% of MgO exhibited high CO_2 adsorption and retention capacity over multiple cycles. In particular, the CaO with 10 wt% MgO exhibited steady adsorption capacity over 30 cycles. Similarly, Wang [96] recently synthesized a porous MgO -stabilized nano CaO powder and realized highly effective long-term conversion because of its resistance to pore-plugging and sintering. Benitez-Guerrero [97] reported the synthesis of porous CaO/SiO_2 composites through a bio-template route using calcium nitrate, $\text{Ca}(\text{NO}_3)_2$, and rice husk as support. The morphology and composition of the biomorphic material improved the CaO multicycle activity, as it served to enhance CaO and inhibited pore-plugging effects. The influence of SiO_2 on CaO/CaCO_3 was also studied by Chen et al. [98]. The optimal 5 wt% SiO_2 -doped CaCO_3 was demonstrated to enhance the reactivity and heat capacity, and led to a 28% enhancement of the reversibility, owing to the rise in grain boundary migration resistance. Table 4 shows the cycling stability achievements of some dopants, adapted from [98].

Table 4. Comparison of cycling stability of CaO/CaCO_3 after doping [98].

Doping Materials	Number of Cycles	Storage Conversion
SiO_2	20	62.09%
Li_2SO_4	11	51.0%
MgO	20	42.03%
$\text{Ca}_3\text{Al}_2\text{O}_6$	20	51.69%

Binary metallic elements and oxides have been experimented with recently. For instance, composites of CaO doped with Mn and Fe were reported to enhance the cycling stability of the TCES material [99]. A synergy between the small grain size and the reinforced skeletal structures prevented agglomeration of the composites, thereby enhancing their cycling stability. On the other hand, Sun et al. [100] reported that 5 wt% Al_2O_3 and 5 wt% CeO_2 co-doped on CaO showed the highest and most stable energy storage capacity under the carbonation pressure of 1.3 MPa during 30 cycles. In addition, the synthetic material possessed strong basicity and provided a large surface area and pore volume during the multicycle energy storage. Again, Raganati et al. [101] experimented with the application of an acoustic perturbation method that remarkably enhanced the carbonation performance of fine limestone particles. Indeed, it prevented agglomeration, which affects carbonation from both the gaseous (CO_2) and solid (CaCO_3) sides of the reaction, thus

enhancing the fluidization quality, reactants' contact, and mass transfer coefficients. More information on in situ data of CaCO_3 doping samples, measurement parameters, and results can be accessed in the work of Moller et al. [102].

Calcium carbonate has the most economic advantage of being widespread, cheap, and having high gravimetric energy density (3029 kJ/kg). The high operating temperatures make this TCES system suitable for various applications such as integration with a solar furnace, and calcium-looping technology. However, this system is stable only up to 20 cycles without any degradation in the absorption capacity. The cycling stability and reversibility must, however, be improved up to 1000 cycles to make this system practical [8].

2.2.5. Deoxygenation/Oxygenation of Metal Oxides

Suitable transition metal oxides undergo a reduction reaction at high temperatures, through which thermal energy is absorbed. The reversible re-oxidation takes place below specific equilibrium temperatures and hence thermal energy will be delivered [103]. Thus, the reversible reduction/oxidation (redox) reactions of metal oxides show high potential as TCES materials. In comparison to the other TCES options, redox systems have the advantage of using air as both the heat transfer fluid (HTF) and the reactant. This eliminates the necessity for a different heat exchanger or gas storage needs. For this reason, TCES based on metal oxide redox reactions permits working with an open system [14]. In this case, it is important to investigate these systems in consistency with the control of oxygen partial pressure (p_{O_2}) [14]. With lowering partial pressures of the reactive gas, the reduction temperature also decreases, as represented in the Van 't Hoff diagram in Figure 6.

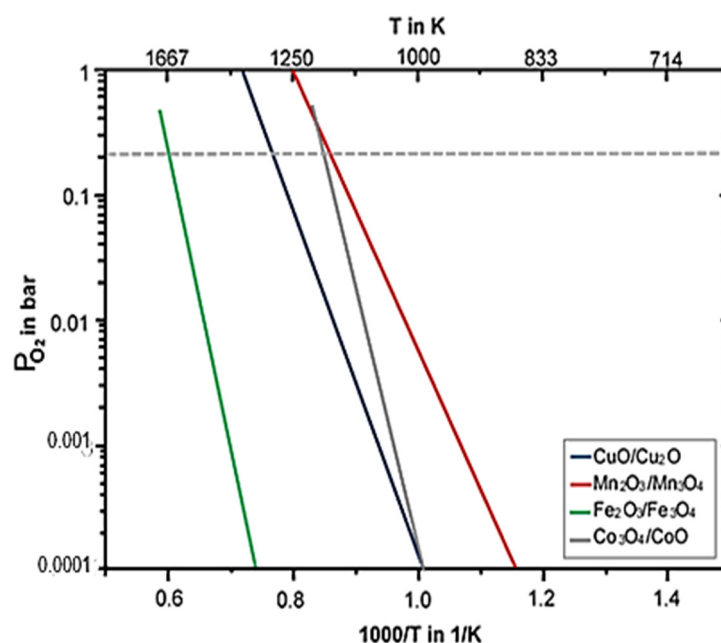


Figure 6. Variation of temperature with oxygen partial pressures for Cu, Mn, Fe, and Co oxides [103].

By comparing metal oxide systems, it was revealed that only cobalt oxide (Co_3O_4), iron oxide (Fe_2O_3), copper oxide (CuO), and manganese oxide (Mn_3O_4) showed befitting reaction temperatures, enthalpies, cycling stabilities, and material costs [103]. In another work, Silakhori et al. [104] assessed the redox reactions of $\text{CuO}/\text{Cu}_2\text{O}$, $\text{Co}_3\text{O}_4/\text{CoO}$, $\text{Mn}_2\text{O}_3/\text{Mn}_3\text{O}_4$, and $\text{Pb}_3\text{O}_4/\text{PbO}$ using TGA. The results showed that $\text{CuO}/\text{Cu}_2\text{O}$ and $\text{Co}_3\text{O}_4/\text{CoO}$ were highly reversible under isothermal pressure-swing cycles, while $\text{Mn}_2\text{O}_3/\text{Mn}_3\text{O}_4$ exhibited slight signs of sintering, and Pb_3O_4 was unreactive up to 550 °C. The free Gibbs energy (ΔG°) was determined for several oxides and PbO_2/PbO , $\text{PbO}_2/\text{Pb}_3\text{O}_4$, $\text{Pb}_3\text{O}_4/\text{PbO}$, $\text{CuO}/\text{Cu}_2\text{O}$, and $\text{Sb}_2\text{O}_5/\text{Sb}_2\text{O}_3$ were confirmed to show thermal storage attributes based on negative ΔG° . Among these, $\text{CuO}/\text{Cu}_2\text{O}$ displayed higher total enthalpy

of 404.67 kJ/mol. However, the occurrence of phase transition was observed at temperatures near 1200 °C, and the molten state is prone to corrosiveness. Deutsch et al. [105] carried out kinetic investigations of the CuO/Cu₂O reaction cycle under isothermal and isokinetic conditions and used simultaneous thermal analysis (STA) and a lab-scale fixed-bed reactor. The outcome of the reaction resulted in substantial discrepancies between both analyses. In STA, outstanding stability of the reaction over 20 cycles was shown with some sintering occurring, whereas heavy sintering occurred in the reactor, which hampered the reaction as well as increased the reaction time three times higher than previously reported values in the literature. Alonso et al. [106] tested the suitability of CuO/Cu₂O in an argon atmosphere and the results indicated the reduction of CuO led to nearly 80% conversion. The reduction in air atmosphere was not favourable because of stronger coalescing particles that hindered the redox reactions. The synthesis of porous CuO-based granules with yttria-stabilized zirconia (YSZ) was also reported [107]. The synthesized granules exhibited high conversion over 100 consecutive cycles in air between 950 and 1050 °C. Stable cycling performances were also obtained in the reactor for 30 consecutive isobaric and isothermal operation modes.

Cobalt and manganese oxides have also been considered promising redox systems for TCES. The CoO/Co₃O₄ system has the potential to be the most suitable pure metal oxide system for TCES due to its fast reaction kinetics and complete reaction reversibility. However, cobalt oxide is also considered potentially toxic and would not be cost-effective for large-scale storage [108]. On the other hand, the Mn₂O₃/Mn₃O₄ redox couple is favoured in terms of minimal cost and toxicity in comparison to its alternatives and has been suggested as an appropriate material for TCES. However, several contentions have been singled out with respect to its capability of full energy storage sustainability with the required number of cycles necessary for this application [109]. In view of this, Bielsa et al. [109] studied several variables such as temperature and heating/cooling rates. A suitable choice of these variables was shown to enhance the heat storage capacity by 1.46 times in a 10-cycle test. The weight-change curves during the TGA are shown in Figure 7, although several levels of sintering were observed, proving the major drawback of this material.

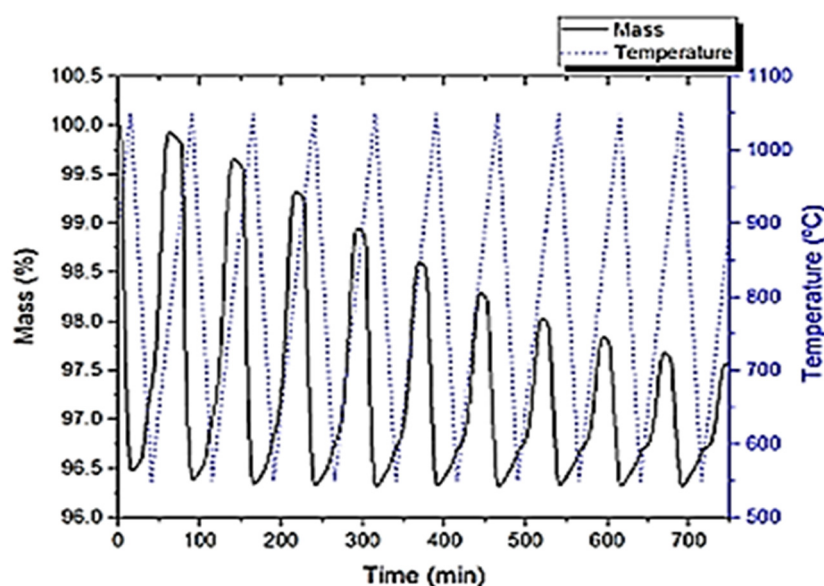


Figure 7. Weight-change curves during 10 Mn₂O₃/Mn₃O₄ TGA cycles between 500 and 1100 °C [109].

Andre et al. [110] studied the impact of Fe, addition which decreased the redox activity and energy storage capacity of Co₃O₄. However, the cycling stability of Mn₂O₃ was significantly improved with added Fe amounts above 20 mol% while the energy storage capacity was unchanged. Similarly, a mixed oxide of Co-Cu-O with low amounts

(<10 mol%) of Cu showed very good cycling stability and higher reaction enthalpy than the others (Mn-Cu-O and Co-Mn-O systems) [108]. Neises et al. [111] performed 30 cycles on a 5 wt% Al₂O₃-doped Co₃O₄ without any material degradation but yielding only a 50% conversion. This was attributed to the insufficient stirring and mixing of the metal oxide particle bed inside the reactor. Notwithstanding, about 400 kJ/Kg energy density was achieved per cycle. The graphical presentation of oxygen absorbed per mol of the doped Co₃O₄ during reduction is shown in Figure 8.

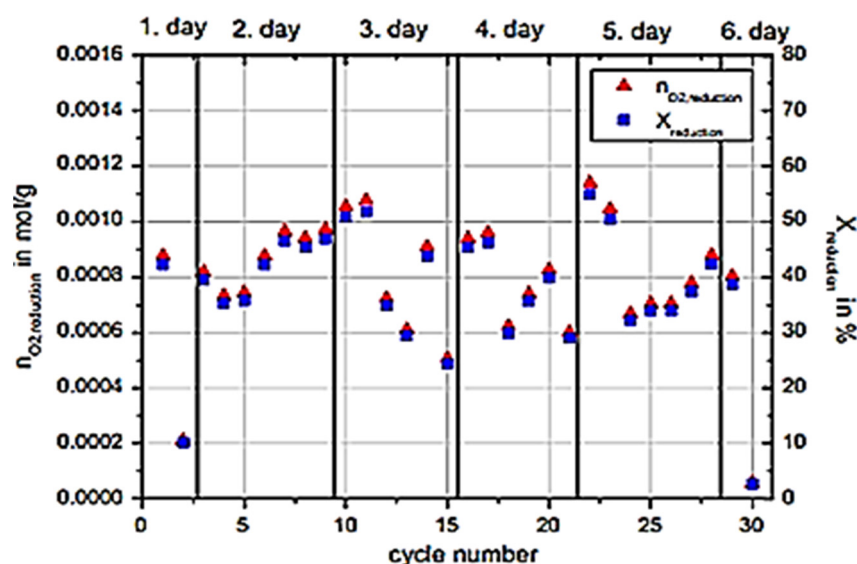


Figure 8. Amount of oxygen per mol of Co₃O₄ and conversion during reduction [111].

In contrast, Carrillo et al. [37] obtained results that indicated that operation with pure oxides (Mn₂O₃ and Co₃O₄) was more effective for TCES application compared to their mixed oxides. Although the values of heat released and absorbed for Mn₂O₃ were far from those obtained with Co₃O₄, its excellent cycling stability, low toxicity, and low cost make it an interesting candidate for heat storage applications. Relatively, the Cu₂O/CuO system has more prospects for TCES application than the CoO/Co₃O₄ system if the reaction is optimized in the reactor. In one experiment [112], isothermal runs at different oxygen partial pressures were carried out with TGA, and defined fractions of CuO samples were analysed. The results revealed that the oxygen partial pressure affects the kinetics, and the reparameterization of the pressure term influences the kinetic analysis of the oxidation reaction. It was concluded that the models described for various parameters provide indispensable prerequisites for the redox reactor designs [112].

So far, this section has presented focused discussions on the various aspects of TCES materials at low, medium, and high temperatures. It is, nevertheless, exigent to present a comparison of some techno-economic parameters of these materials, as summarized in Table 5. The materials in the table are representative candidates according to each temperature domain and could help in making preliminary considerations for suitable technology.

Table 5. Comparison of cost, efficiency, and charge/discharge cycles of TCES materials.

Material	Reaction Temperature (°C)	Energy Density (kJ/kg)	Price (\$/kg)	Conversion Efficiency (%)	Number of Cycles	Reference
MgCl ₂ ·6H ₂ O	130	940	0.18	87	25	[22,113]
MgH ₂	300–480	2160	800–900	20	20	[8,12,22,113]
Ca(OH) ₂	400–600	2000	0.1–0.18	49	100	[8,20,113]
CaCO ₃	973–1273	3029	0.2–2.05	27.3	30	[8,9,12,22,113]
Co ₃ O ₄	863–896	844	10–20	70	30	[8,104,113]

Ferchaud et al. [114] demonstrated that the heat stored (0.84 GJ/m^3) and released (0.71 GJ/m^3) in $\text{MgCl}_2 \cdot 6\text{H}_2\text{O}$ was, respectively, 79% and 87% in the storage cycle. The small difference in the charging/discharging heat was attributed to the textural changes in the material. In another TGA/DSC test, the $\text{MgCl}_2 \cdot 6\text{H}_2\text{O}$ material showed a 40% lower heat output after 25 cycles and a further 10% drop at the 28th cycle, compared to the first [115]. An open sorption system using $\text{MgCl}_2 \cdot 6\text{H}_2\text{O}$ has also been tested, but the lower heat-recovery efficiency resulted in a power loss of nearly 70% [116]. It is common knowledge that the actual energy density obtained from experimental prototype tests differs significantly from the theoretical energy density [59].

For MgH_2 , a multicycle system has been reported [117], where cycle 1 represented the activation phase at around $300 \text{ }^\circ\text{C}$. The desorption kinetics showed a slight improvement from cycle 4, and stabilized in cycles 6–8 with 90% storage efficiency. However, performance degradation of the system was noticed after 10 cycles with a storage capacity reduction of 50% after 20 cycles. However, a solar-heated MgH_2 material at $420 \text{ }^\circ\text{C}$ showed the metal hydride to be thermally cycled more than 20 times with a minimal loss in hydrogen capacity [118]. A coupled TGA study of a modified MgH_2 powder also reported a cyclic conversion of 98.4% after 30 full cycles, with a calculated degradation rate of 0.00043 wt\% per cycle [119].

In TGA experiments, a remarkable 100% conversion efficiency and cycling stability of $\text{Ca}(\text{OH})_2$ has been proven over 100 cycles up to 95.6 kPa vapour pressure [78]. However, only 32 charge/discharge cycles could achieve 100% conversion efficiency at 100 kPa due to material structural failure [80]. Yan and Zhao [120] analysed the charging/discharging characteristics of $\text{Ca}(\text{OH})_2$ and showed that heat storage efficiency increased with temperature (47% at $510 \text{ }^\circ\text{C}$ and 65% at $540 \text{ }^\circ\text{C}$). However, higher heat-release efficiency could be achieved by reducing the temperature and increasing the vapour pressure. In particular, the conversion was 31.7%, 60.9%, and 72.8% under vapor pressures of 180 kPa , 240 kPa , and 320 kPa , respectively.

Generally, pure CaCO_3 does not show complete reversibility during decarbonation/carbonation cycles due to pore-plugging effects [9]. The best performance reported a 40-cycle high-temperature carbonation/decarbonation run. The initial cycle was always 100%, but the cyclic conversion progressively decreased due to the loss of pore volume [9]. A recent study on the multicyclic stability of different CaCO_3 minerals showed a limitation after 20 conversion cycles [97]. A comparative study of a sulphate-modified CaCO_3 found a 51% cyclic conversion over 11 decarbonation/carbonation cycles, which was higher than the 27.3% of pure CaCO_3 [121]. Thus, the addition of inert materials is seen as a viable option for improving the cycling stability of the CaCO_3 . This is proven by CaO multicycle conversion data for different pretreated samples over 20 carbonation/decarbonation cycles carried out under calcium-looping-concentrated solar power (CaL–CSP) storage conditions.

For Co_3O_4 , TGA results show rapid full thermal reduction and complete weight recovery for CoO oxidation to Co_3O_4 [11]. Hutchings et al. [122] reported 100 cycles of Co_3O_4 between $870 \text{ }^\circ\text{C}$ and $955 \text{ }^\circ\text{C}$ with 99% conversion efficiency and no evidence of degradation under these conditions. Again, Co_3O_4 powders exhibited long-term (30 cycles) performance with complete and reproducible cyclic redox performance within the temperature range of $800\text{--}1000 \text{ }^\circ\text{C}$ [123]. It has been observed that TGA results generally show higher oxidation fractions with lower cooling rates. Neises et al. [111] tested the solar-heated redox reaction of Co_3O_4 for 30 cycles in an integrated system and achieved a storage density of 400 kJ/kg per cycle. The system was only limited by insufficient mixing of the material.

3. Thermochemical Energy Storage Reactors for Solid–Gas Reactions

Reactors provide the platform for the operation of thermochemical storage systems. To guarantee efficiency in the charging and discharging process of the TCES material, an innovative reactor concept fashioned for particular operation and storage material is necessary [124]. That is, the nature of reactants or the type of reaction determines the type and design of the reactor and the system integration. Additionally, the art of designing

efficacious reactors is as important as material enhancement itself. Different criteria have been used to classify reactors, such as operation mode, number of phases, reaction types, or a combination of these [125]. Based on the mode of operation, three major solid–gas reactors are implemented: fixed (packed)-bed, moving-bed, and fluidized-bed reactors [8], as shown in Figure 9.

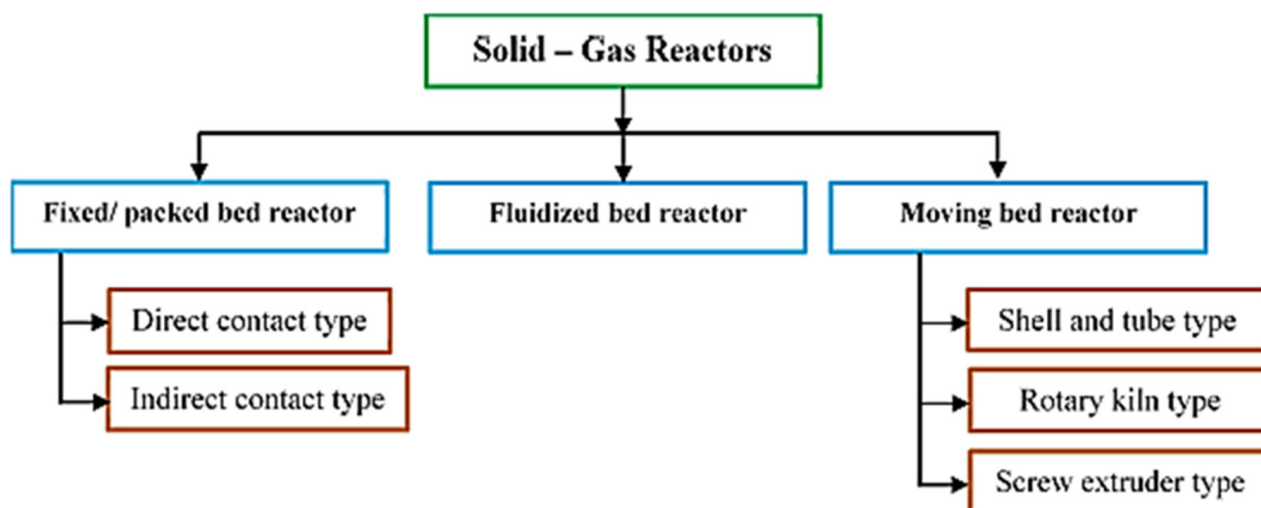


Figure 9. Classification of solid–gas reactors [8].

3.1. Fixed-Bed Reactors

Fixed or packed beds are hollow tubes, pipes, or other vessels filled with packing materials for chemical processing. The packing material may contain catalyst particles or adsorbents, and the purpose of such a bed is to improve contact between two phases in a chemical process. Thus, in packed-bed reactors, the solid reactants/products are arranged in the vessel's bed during heat storage and release, with the flux of reactants passing through the stationary bed. The HTF and reactants are not in contact with each other, resulting in heat transfer through the walls of heat exchangers.

Fixed-bed reactors are the most common lab-scale test rigs and have been investigated by Schmidt et al. [126]. In this work, several dehydration and hydration cycles were performed to study the charge and discharge characteristics of a 20 kg $\text{Ca}(\text{OH})_2$ material. The dehydration was performed at 45 °C and the rehydration at about 55 °C. A conversion of 77% without degradation after 10 cycles was achieved. Investigation of different charging and discharging temperatures was then recommended to optimize the overall conversion of the material. Again, Ranjha et al. [127] modelled a two-dimensional rectangular bed filled with $\text{CaO}/\text{Ca}(\text{OH})_2$ powder for different flow geometries and bed properties. They showed that increasing the porosity of the bed provided higher energy density but slowed the reaction, resulting in a lower average outlet temperature. A possible remedy for this deficiency would be to increase the bed dimensions, but this could result in a slower reaction owing to the poor thermal conductivity of the materials. This suggests that a systematic optimization process could be applied as a compromise between various parameters. However, this depends on the desired output temperature, energy requirements, and the rate of thermal energy storage and retrieval. Figure 10 shows the results of comparing varying bed porosities with total conversion time and the maximum outlet temperature in counter-current flow geometry.

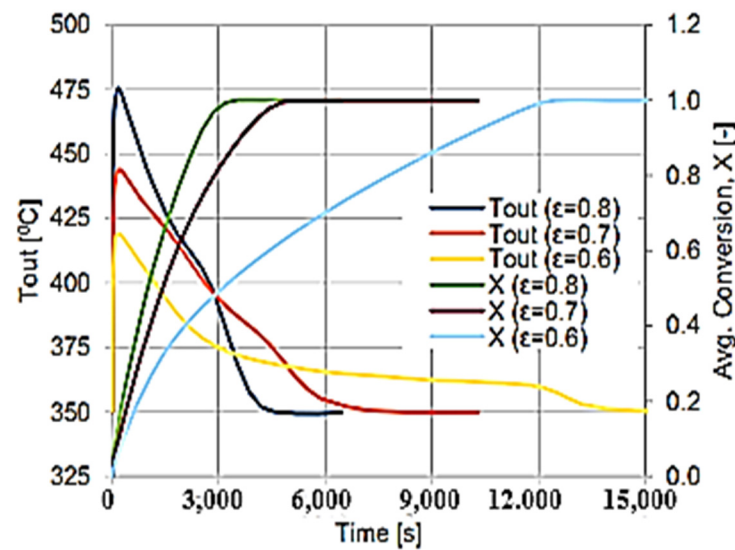


Figure 10. Outlet temperature of the HTF and the conversion as a function of time during hydration for bed porosity of 0.6, 0.7, and 0.8 in counter-current flow geometry [127].

On the other hand, Funayama et al. [128] evaluated a 60 g $\text{Ca}(\text{OH})_2$ pellet in a packed-bed reactor. The heat storage density of the bed was 1.0 MJ/L-bed, and an average heat output rate of 0.71 kW/L-bed was observed for the first 10 min under a hydration pressure of 84.6 kPa. Although the bed showed a net expansion and formation of agglomerated lumps in the middle, the effects had a small influence on the reactivity. The stability of the reaction conversion of the bed was demonstrated during 17 cycles of experiments. Figure 11 shows the experimental setup for the test rig.

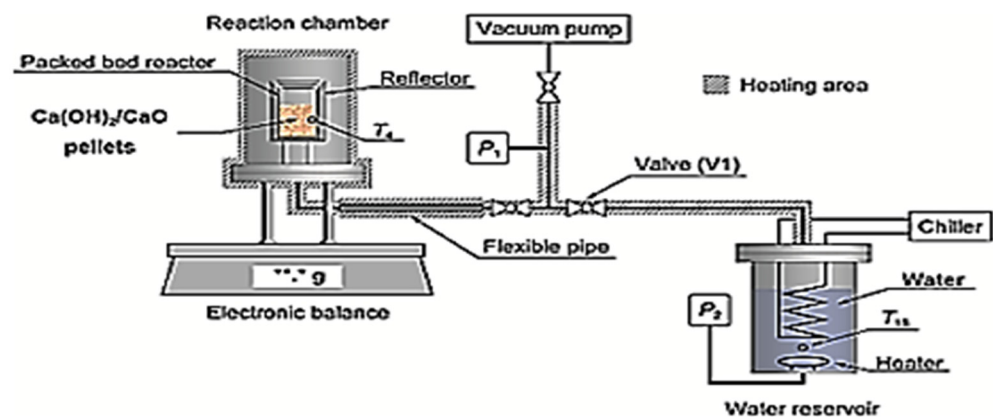


Figure 11. Schematic diagram of the experimental setup in Funayama et al. [128].

It is established that the heat transfer coefficients in indirectly heated fixed beds are generally limited by the low thermal conductivity of the reactants [129]. Therefore, a fixed-bed reactor in indirect operation at varying technical operating conditions was investigated by Schmidt et al. [130]. Thermal charging and discharging were experimentally demonstrated at vapour pressures between 1.4 kPa and 20 kPa. This indicated the possibility of operating the system at low vapour pressures, thus raising the total efficiency of the storage system. However, the range of operation of the $\text{Ca}(\text{OH})_2$ system was constrained because of its efficient rate of reaction at low vapour pressure. Again, Peng et al. [131] simulated fixed-bed reactors under various operating conditions, and the impact of key process parameters was evaluated. An optimized model for the design was then used to compare the performance of three TCES reactors for Mn_2O_3 , $\text{Ca}(\text{OH})_2$, and CaCO_3 . The results showed CaCO_3 and $\text{Ca}(\text{OH})_2$ had more favourable conversion efficiencies.

Moreover, the HTF inlet and outlet temperature profiles also indicated the two aforementioned reactors rapidly reaching the endothermic reaction temperature. These results are shown in Figure 12.

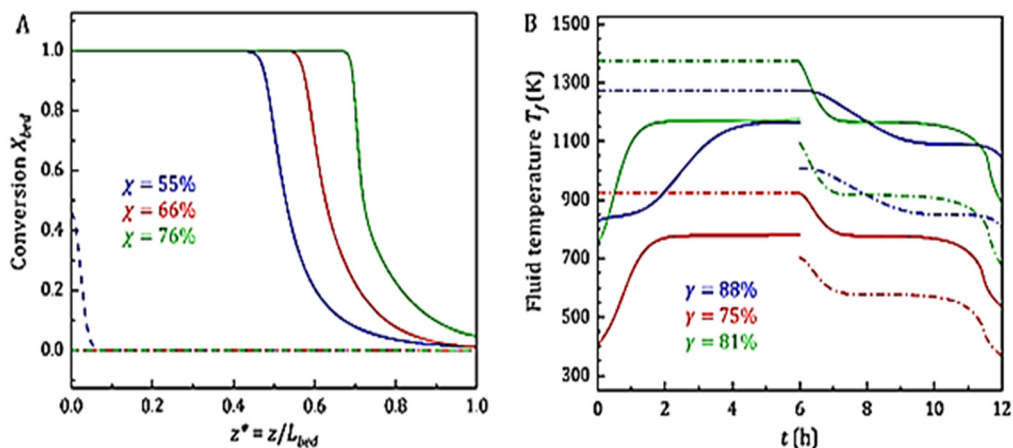


Figure 12. (A) Bed conversion efficiency and (B) fluid temperature of fixed-bed reactors. In (A), conversions at the start of charging ($t = 0$) are shown as dashed lines, and those at the end of charging ($t = 6$ h) as solid lines. In (B), fluid temperatures at the inlet are shown as dash-dotted lines, and those at the outlet as solid lines (blue: Mn₂O₃, red: Ca(OH)₂, green: CaCO₃) [131].

On the other hand, Schaubé et al. [132] earlier investigated a reactor with direct heat transfer for the CaO/Ca(OH)₂ material. The simulated results of a 2D model developed showed good agreement with experiments. However, deviations were observed in temperature characteristics with an increasing flow rate of the HTF. This was due to the overestimation of the reaction rate. To forestall this in further research, a derived kinetic equation would be adapted to the actual conditions, for instance, particle size, to account for diffusion limitation. Then, the developed model could be used to predict the performance of a reactor with direct or indirect heat transfer.

Therefore, integrating these heat storage systems into industrial processes needs additional theoretical and experimental investigations [28]. Improving the low thermal conductivity, for instance, in an indirectly heated fixed bed requires a large heat exchanger, which adds cost. One way to surmount this challenge is to separate the heat exchanger (power) of the costly reactor from the storage material (capacity). A moving-bed concept in which the material moves through the reactor could be used to accomplish this [133].

3.2. Moving-Bed Reactors

In moving-bed reactors (MBRs), the bed can be shuffled in continuous or regular intervals in portions, and the flow of fluid is similar to what happens in a fixed bed. Moving-bed reactors were thought to have the advantage of improving thermal conductivity through enhanced solid–gas particle interaction. These solid–gas reactors can be categorized into two different regimes: (i) the axial-flow regime (concurrent and counter-current) and (ii) the crossflow pattern [134]. For instance, in the axial-flow solid–gas moving bed configuration, the advantages of the counter-current flow regime have been applied through the direct interaction of reactants. In this case, the solid flows downward while the gas moves upward as the chemical transformation occurs.

Notably, fine powders were observed to have very low flowability [135]. To improve this, a 1D simulation of a manganese-iron oxide (Mn-Fe oxide) TCES reactor was investigated [136]. An extension of the particle flow model was simulated for a counter-current MBR, and complete conversion was attainable only for low gas as well as low rates of solid flow. Thus, the oxidation kinetics of the redox transition was the limiting factor. Moreover, a contrasting trend was observed in which the energy density dropped, although the thermal

power surged independently of the attained conversion efficiency in the given conditions of operation. (See Figure 13). Additionally, sensitivity analyses revealed the possibility of channels developing within the moving bulk material, which could slow down the heat transfer between solid and gas. Hence, a proposal for direct and indirect heat transfer coupling was recommended as a promising operational mode.

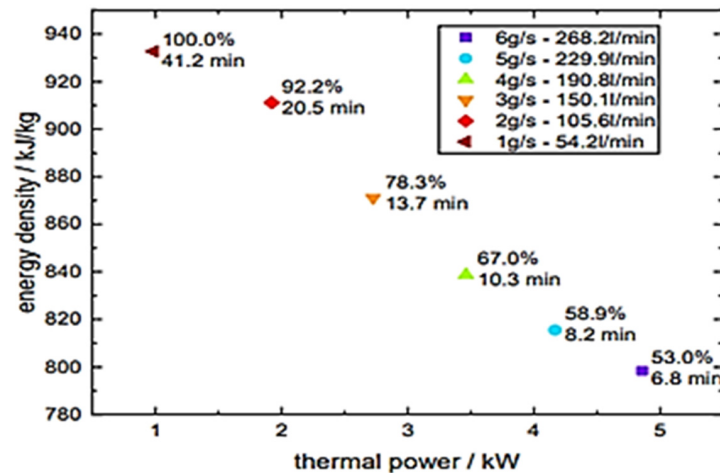


Figure 13. Thermal power of the MBR for the steady-state case and energy density of the material with different particle and gas flow rates [136].

Furthermore, Preisner and Linder [137] investigated the reaction behaviour of manganese-iron oxide (Mn-Fe oxide) at different temperatures and pressures. The TCES material was oxidized to an extent of 80.2% after a previous reduction of 77.1% at 20 kPa oxygen partial pressure. Moreover, a sufficiently stable oxidation/reduction reaction was established for two successive cycling tests (of 30 cycles each) in TGA. However, the flowability of the material particles was limited at high temperatures between 850 and 1050 °C due to mass loss, as shown in Figure 14.

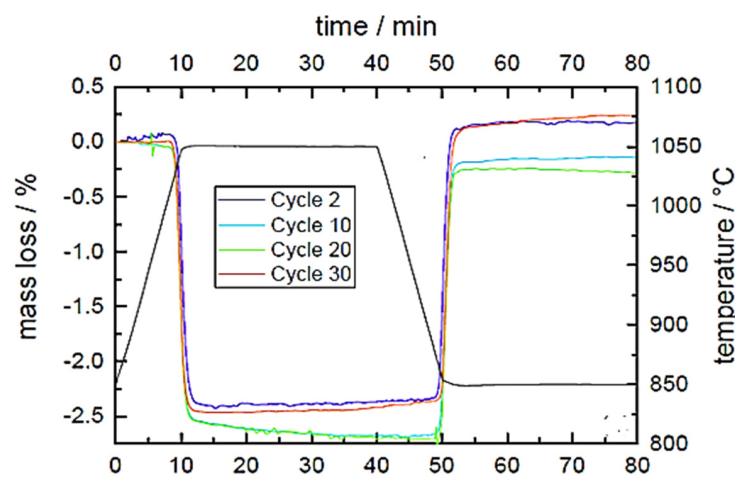


Figure 14. Relative mass loss of the Mn-Fe oxide during the first 30 redox cycles [137].

Huang et al. [138] investigated the complex physical and chemical transport phenomena in MBRs. The coupled heat/mass transfer and reactions were successfully modelled based on uniform flow and plug flow. Both models showed potency for simulating the transient flow processes. In particular, the plug flow model based on Ergun's equation successfully predicted the increased gas velocity inside the reaction zone. However, due to a lack of exact information on the heat flux input during the transient phase, the reaction zone temperature was overpredicted, and this led to overestimated oxygen concentration

at the exit. In another concept, a rotary kiln was also tested for suitability in a thermochemical storage process [106]. Rotation movement helped to improve the reactivity of the sample by mixing the particles. However, the reaction was handicapped because of strong coalescing particles. Additionally, the chemical conversion was significantly lower for oxidation than for reduction. For this reason, optimization of the operation parameters such as rotational speed, particle size, gas flow, and initial mass of reactant was recommended. This would increase the conversion of both reduction and oxidation and avoid the progressive loss of reactive fraction. So far, no successful operation of a moving-bed reactor over multiple cycles has been reported [135].

3.3. Fluidized-Bed Reactors

For fluidized-bed reactors, the fine solid particles are sustained in suspension by the fluid's upward flow [57]. Essentially, the base of a fluidized bed is similar to that of a fixed bed. With the increase in the fluid velocity, the solid particles are suspended at the minimum fluidization velocity. Better heat and mass transfer can be accomplished with fluidized-bed reactors (FBRs). FBRs require significantly lower gas velocities [135], therefore, they have been extensively suggested for more efficient TCES. However, getting the material fluidized, which in turn demands a huge increment in gas flow volume, has the consequence of decreasing the efficacy of the stowage mechanism. Notwithstanding, the advantages of fluidized beds over other reactors include better reaction efficiency due to enhanced fluid-particle interaction. Again, besides the limited pressure drop across the bed, fluidized beds efficient HAM transfer from the continuous particulate interactions and higher transfer coefficients [139]. In addition, the uniform temperature gradient ensures the elimination of dead zones and hot spots. A comparison of the three solid-gas reactors is summarized in Table 6.

Table 6. Comparison of fixed-, moving-, and fluidized-bed reactors [24].

Reactor	Advantages	Disadvantages
Fixed/Packed bed	<ul style="list-style-type: none"> Easier modelling 	<ul style="list-style-type: none"> Low heat and mass transfer High-pressure drops
Moving bed	<ul style="list-style-type: none"> Direct solid-gas heat transfer 	<ul style="list-style-type: none"> Complex hydrodynamics
Fluidized bed	<ul style="list-style-type: none"> Minimization of hotspots and thermal instability High heat transfer coefficients 	<ul style="list-style-type: none"> Complex hydrodynamics and modelling Internal component erosion

Generally, TCES technology is still at the infancy level, notwithstanding the increasing investment in research. So far, no known commercialization project has been launched, but a number of lab-scale projects and, in some cases, prototypes are reported [26]. We, again, present a focused outlook on the technology status of the potential TCES systems in the low to high-temperature range (Table 7).

Table 7. Examples of TCES system prototypes and projects.

Reference	Storage Material	Technology	Description
Zondag et al. [140]	MgCl ₂ ·6H ₂ O	Packed bed	<ul style="list-style-type: none"> Prototype for solar heat storage Produced heat for 40 h Power transfer efficiency of 33%
Delhomme et al. [141]	MgH ₂	Tank rig	<ul style="list-style-type: none"> Reactor coupled to an industrial heat source Degradation after 10 cycles Achieved 60% efficiency

Table 7. Cont.

Reference	Storage Material	Technology	Description
Schmidt et al. [126]	Ca(OH) ₂	Fixed bed	<ul style="list-style-type: none"> ■ Reactor with indirect heat transfer ■ Achieved 10 stable reversible cycles ■ Attained 77% efficiency and 10 kW power
Meier et al. [142]	CaCO ₃	Rotary kiln	<ul style="list-style-type: none"> ■ Solar-heated moving-bed reactor ■ Achieved 90–98% conversion rate ■ 10 kW power; thermal efficiency of 20%
Neises et al. [111]	Co ₃ O ₄	Rotary kiln	<ul style="list-style-type: none"> ■ Solar-heated prototype reactor ■ Achieved 30 stable cycles with 90% efficiency

It can be seen that current projects or prototypes involve mainly packed (or fixed) beds and moving beds (rotary kilns). Fixed-bed reactors can be operated continuously, are cost-effective, and offer high reaction conversion per unit mass of material. A rotary kiln, on the other hand, serves to raise materials to high temperatures. The rotation of the vessel ensures a continuous movement of materials between the entrance and exit of the kiln. In the literature, fixed-bed and moving-bed prototypes have a reactor efficiency of between 12 and 69%, whilst the whole (integrated) system efficiency is between 12 and 42% [21]. In terms of the overall cost of TCES technology, a probabilistic analysis is necessary to account for the variability and uncertainty of transient factors [143]. A method to estimate the capital costs and the profitability of TCES systems has been developed by Flegkas et al. [144].

Designing a gas–solid reactor is influenced by three factors: reaction system kinetics, particle size sequence, and particle flow model for solid and gas in the reactor [57]. This supposes a requirement for system modelling to deepen understanding and help in the simulation of processes. Moreover, the research effort is currently aiming to gain new insights into the reactants' basic molecular level, as well as scale up improvements and optimization of fluidized beds [139]. Admittedly, the modelling of these systems is complicated, and more so when storage materials are to be included. Many researchers have carried out work on the modelling of physical phenomena in TCES reactors. Thus far, numerical or experimental efforts have rarely investigated the physical and chemical processes at the particle scale [28]. Moreover, it is only recently that energy and exergy analyses on conceptual thermochemical heat storage systems are being implemented.

Flegkas et al. [145] proposed a method to model FBRs based on solid-state kinetics and fluidization hydrodynamics, using the MgO/Mg(OH)₂ reaction couple. The reaction enthalpy dropped significantly using water, hence the supply of steam constituted the main drawback. In another work, Angerer et al. [135] proposed a reactor concept featuring a bubbling fluidized bed with continuous, guided solid flow and immersed heat exchanger tubes. Fluidization of the CaO/Ca(OH)₂ powder proved herculean, but challenges were surmounted with the use of mild calcination settings and a peculiarly designed gas distributor plate. Analyses revealed that heat transfer between the reactor and the immersed heat exchangers had the largest influence on the system performance. The results of the first steady-state experiments in a new power plant implemented to investigate the idea under practical reactor conditions were reported by Rouge et al. [146]. The basic conceptual scheme of the integrated system is shown in Figure 15. The experimental results during dynamic and steady-state periods were fitted to a KL reactor bubbling-bed model. The reactor performance modes were sufficiently predicted by the model, as observed during the experiments under dynamic and steady-state conditions. This model would be a relevant tool for the future expansion of this energy storage technology.

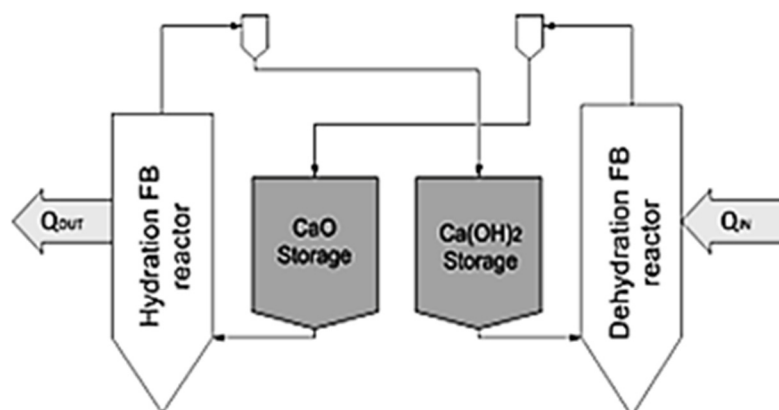


Figure 15. Basic conceptual scheme of the CaO/Ca(OH)₂ energy storage system [146].

In addition, Mu et al. [147] carried out a numerical simulation study of the thermal behaviour and hydrodynamics of FBR using the computational fluid dynamics-discrete element method (CFD-DEM). The effects of superficial gas velocity, bed height, and heat source distribution were analysed. The results showed that both the gas superficial velocity and the bed aspect ratio had a profound influence on fluidization behaviour and temperature distributions. Figure 16 shows the voidage as a function of the superficial velocity and aspect ratio. This work is similar to that of Hawwash et al. [18], in which the reactor design and area ratio were shown to impact the thermal performance and energy storage during the dehydration of a TCES material.

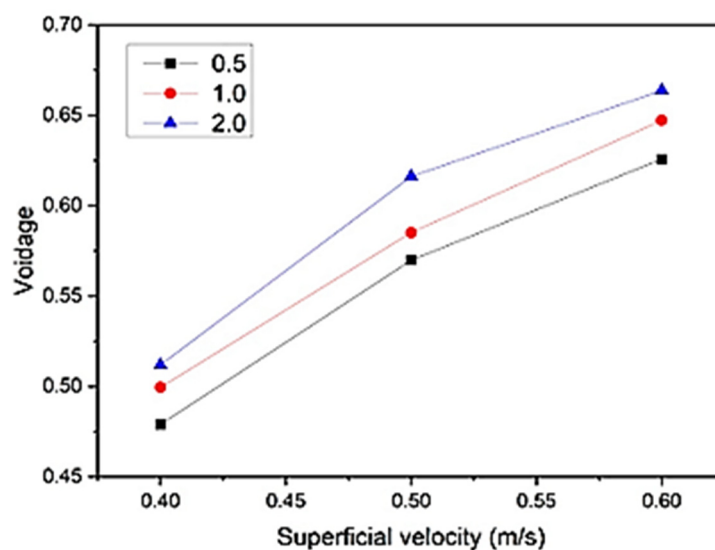


Figure 16. Temporally and spatially averaged bed voidage as a function of superficial velocity and aspect ratio [147].

Despite these milestones in understanding reactor dynamics, technical barriers still exist in conventional thermochemical energy storage systems. Efforts to enhance reactants with various additives or using different geometries of reaction beds have not abated the dynamic limitations of HAM transfers. For this reason, Darkwa et al. [148] proposed and investigated an agitated fluidized-bed reactor system. The model revealed substantial improvements in adsorption capacities and enhanced heat transfer rates. However, the thermophysical variables that influenced the minimal fluidization velocity in the adsorption column needed to be optimized. This would be necessary for efficient exothermic reaction and thermal exchange. The effect of agitation on the fluidization characteristics of fine materials was validated with different materials. Kim and Han [149] used fine particles

(22 μm) of material in a fluidized bed. The agitator was of the pitched-blade turbine type. The results showed that smoother fluidization was achieved with increasing agitation speed. Additionally, agglomeration and channelling were reduced by the mechanical effect of the agitation. Spectral analysis of the pressure drop fluctuation had the shape of a short-term correlation with different agitation speeds (See Figure 17). The void fraction also increased with the increasing speed of agitation at the constant fluidizing gas velocity, as shown in Figure 18.

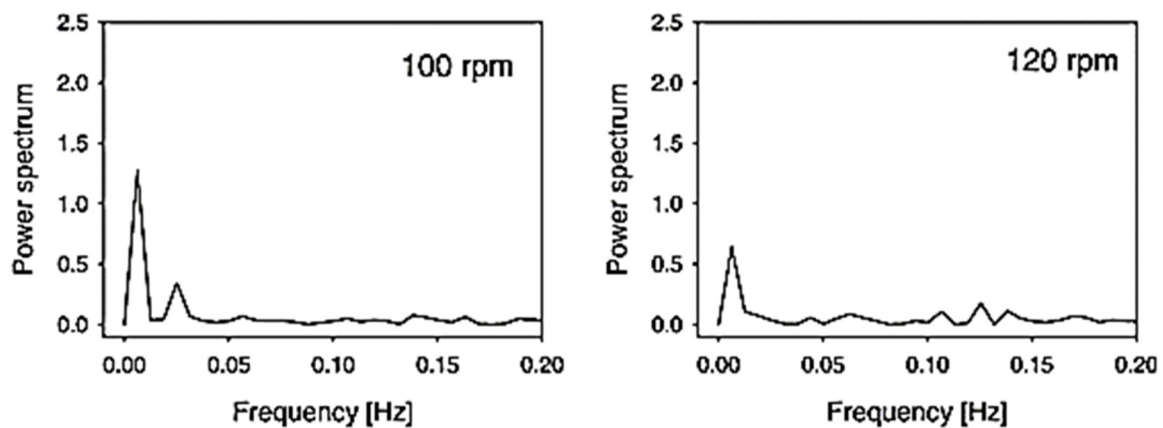


Figure 17. Power spectrum of the bottom zone of the bed for different agitation speeds [149].

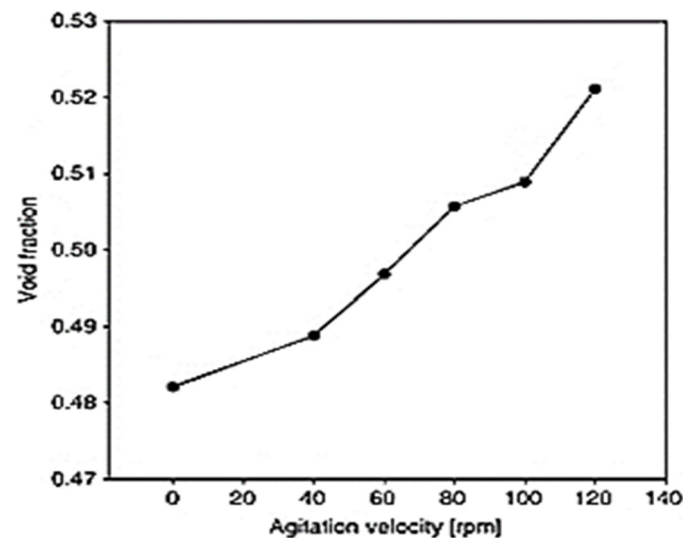


Figure 18. Graph showing an increase in the void fraction of powder material with agitation speed [149].

Again, the effect of agitation on fluidization in a solid–gas fluidized-bed reactor with a frame impeller was studied using a 3D unsteady CFD method [150]. The numerical method combined a two-fluid model and the kinetic theory of granular flow. The results showed that a substantially high agitation speed yielded higher performance in fluidization in addition to reduced bubble diameters and internal circulations of particles. Lv et al. [151] also reported the effectual performance of a fluidized bed under mechanical agitation, where the symmetrical motion pattern of the bed particles was identified. Similarly, the bubble diameter was also significantly reduced with increasing agitation speed, as presented in Figure 19. Furthermore, encouraging results showing the reduction in entrainment rate and channel flow and enhanced particulate interaction have been reported with an arch agitator [152]. Again, using a 3D CFD model, Shi et al. [153] established strong evidence

of improved fluidization efficiency and reduction in the operation stability of a solid–gas fluidized bed.

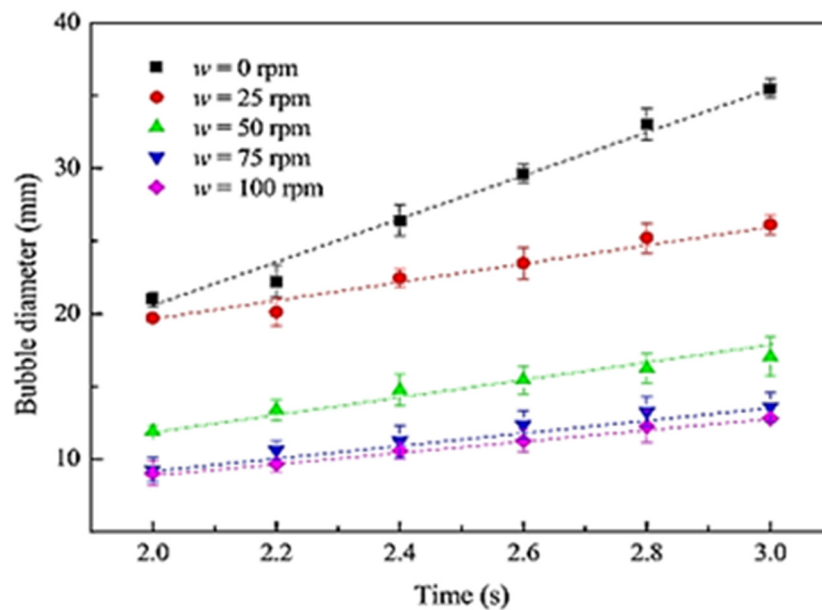


Figure 19. Graph of variation of bubble diameter with agitation speed [151].

A variety of reactor types have been developed, as found in the reviews of [19,28]. A concise summary of different reactor classifications, descriptions, and reactor and/or integrated system efficiencies is available in the review by Gbenou et al. [21]. Much research effort has been devoted to the development of thermochemical reactors, but few laboratory prototypes have been tested in large-scale pilot projects. In a recent review [26], the low technology-readiness level of TCES was attributed to the cost or performance of materials and reactor design. To improve on this rating, the reviewers canvassed a shift from microscopic views of numerical design processes to macroscopic comprehension of reactor design and analysis. Their paper, therefore, focused on low-temperature reactors and, again, reiterated the promise of FBRs. One significant highlight of the work was a proposal for computational resources (COMSOL Multiphysics and TRNSYS software) for the visualization of reactor phenomena for a better understanding of the transient processes.

4. Overview of Modelling and Simulation in TCES Systems

Modelling and simulation have the potential to improve understanding of the complex phenomena in TCES, either at the level of the material or in integrated systems. So far in this review, a good number of numerical studies have been cited. However, this section is intended to give an overview of the modelling and simulation approaches being explored by researchers for insights, analysis, or validation in thermal storage experiments. In the last couple of years, numerical modelling tools have been increasingly used, and the growing capability in computational power is increasing in reliability and accuracy, as well as lowering the time and cost invested in traditional experiments. Already, research efforts are currently aiming to gain new insights at the reactants' basic molecular level as well as scale up improvements and optimization of fluidized beds.

At the level of the material, for example, TCES can benefit from the achievements of molecular dynamics (MD) simulations in establishing good knowledge of thermophysical properties in materials such as phase change materials (PCMs) [154]. In particular, MD simulation with LAMMPS (Large-Scale Atomic/Molecular Massively Parallel Simulator) code has proven to be a capable tool for calculating the trajectories of particulate interactions in materials under some boundary conditions, and there is the possibility of obtaining desired thermodynamic information. For instance, to adequately decipher the

metastability in a nitrate/MgO system regarding charging and discharging reactions, Shkatulov et al. [155] carried out MD simulation of LiNO_3 -doped $\text{Mg}(\text{OH})_2$ and pure $\text{Mg}(\text{OH})_2$ systems to understand the difference in equilibrium temperatures for the dehydration process. The results showed striking proximity of the theoretical and experimental values. Again, agglomeration is one of the recurring challenges, especially in TCES with powder materials. In a quest for deeper insight into its occurrence, simulations of the agglomeration behaviour of the $\text{CaO}/\text{Ca}(\text{OH})_2$ system were carried out [156]. The results revealed that the agglomeration rate was slower during discharge cycles of CaO in the presence of H_2O . In addition, the introduction of silica (SiO_2) particles into CaO was shown to effectively subdue agglomeration of the reactants. Thermophysical properties of CaO have also been investigated by Alvares et al. [157]. The obtained theoretical results provided accurate perspectives for calculating the thermodynamic properties in a temperature region difficult to access through experiments.

In complementarity to the atomistic scale simulation of TCES materials, suitable reactor concepts such as FBRs also require optimization of HAM flow, modelling, and simulation of the impact of transient effects. A large body of literature employs a variety of CFD-based models for the analysis and prediction of processes in fluidized-bed systems. The CFD-DEM model has been used to study the thermal behaviour and hydrodynamics in FBRs [147,158]. In one work, the fluidization velocity and bed aspect ratio impacted the temperature distribution [147], indicating that multiphase flow influences heat transfer in the FBR. In another, the particle size, density and bubble formation essentially affected the thermochemical properties of the fluidized material [158]. Shen et al. [159] carried out a feasibility study of a solar-integrated fluidized bed employing the CFD Eulerian model using ANSYS-FLUENT. Analysis of the results showed robust performance of the bed at high operating temperatures, but stabilization of the outlet temperature was required for optimal yield. Similarly, a 2D axisymmetric model of the Eulerian type was used to investigate the $\text{MgO}/\text{Mg}(\text{OH})_2$ system [160]. The bed temperature was shown to be unaffected by the efficiency of the heat transfer, but the reactor throughput was limited by the kinetics of the hydration reaction. Essentially, the rate of gas flow and bed expansion ratio largely impacted the system heat stowage. The numerical results were validated experimentally by investigating the energy flow and dissipation optimization in the FBR. TRNSYS was also used by Li et al. [161] to test the $\text{MgO}/\text{Mg}(\text{OH})_2$ system for solar thermal stowage. Analysis of the simulated charging/discharging phases of the TCES system indicated a contribution of 94.6% of the heating demand during the exothermic phase. Furthermore, AspenPlus was used to design, model, simulate, and optimize a combined charge/discharge process for a $\text{CaO}/\text{Ca}(\text{OH})_2$ system coupled with concentrated solar power [162]. A sensitivity analysis of the results of the fluidized-bed-based process flowsheets was comparable to the reported models in the literature.

Although a plethora of literature exists on different models applicable to various fluidized bed systems, CFD provides a vast array of tools. In a comprehensive state-of-the-art review of CFD methods, Alobaid et al. [163] described the CFD-DEM model as becoming formidable if coupled with chemical reactions and HAM transfer, yet still requiring upgrading to be competitive. In particular, CFD-DEM simulations are reported to be computationally costly in tracking an avalanche of particles in solid-gas flows requiring the detection of particle-particle and particle-wall collisions. According to the reviewers, two-fluid models, for example, ANSYS-FLUENT, have the advantage of flexibility in the implementation of new algorithms and chemical or physical models, such as in the implementation of the so-called user-defined function (UDF). The major challenge with fluidized-bed modelling lies in the nonlinear and nonequilibrium behaviour of the solid-gas flows [163]. This implies a requirement for a combination of more than one model in the modelling and/or simulation processes. In this review, we emphasize the need to harmonize efforts from the viewpoint of material development processes to conceptual reactor design issues, by modelling and simulating the integrated systems. A specific potential material of interest could be enhanced according to its identified limitations and

intended application. Molecular dynamics (MD) simulations, especially with LAMMPS code, can give useful numerical details of the kinetics and thermodynamics of the reactions. This molecular scale insight will be of enormous help in obtaining useful physical parameters for reaction conditions, design, and optimization of suitable reactor systems. MD simulations of this nature are, therefore, recommended for various TCES materials of interest in the desired temperature range of applications.

For the reaction bed, it is auspicious that HAM flow optimization, modelling and simulation of transient effects, and the charge/discharge reaction kinetics, among others, can be investigated in the FBR. We propose that modelling and simulating the FBR with an incorporated agitator mechanism will be a novel approach to enhancing HAM transfer coefficients via rigorous particulate interactions and shortened residency times. Together with a suitable heat exchanger framework, the overall efficiency of the system will be raised. The reactor geometry and the physical phenomena occurring within it could be visualized using capable computational tools such as AspenPlus software. There are good prospects for modelling such a transient state with ANSYS-FLUENT that can couple the multiphase flow and chemical reaction, on the premise of the Eulerian-Eulerian model, heat transfer, and kinetics equations. The influence of bed and fluid flow dynamics on thermal storage and release could then be established upon analysis of the reaction processes.

5. Conclusions

This review looked at research efforts in TCES from the viewpoint of energy storage materials to reactor systems. The work mainly focused on numerical and experimental studies carried out on promising storage materials from low to high temperatures. Additionally, the three conventional solid-gas reactor concepts, namely fixed-bed, moving-bed, and fluidized-bed reactors were reviewed. Metal hydroxides and metal carbonate systems, especially Ca-based, are currently under renewed investigation. Their attributes of high energy densities, relative cheapness, and non-toxicity have encouraged interest in developing compact and low-cost systems for industrial waste heat utilization.

Most promising materials investigated still suffer from agglomeration and low thermal conductivity, which has limited their performance in the reactor. Efforts have been made to improve the properties of the materials with various additives with some levels of success, but the problems of poor mass and heat transfer in different reactor configurations have remained. Coupled TGA-DSC procedures have been employed to characterize TCES materials, and these can be helpful for preliminary material selection. Nonetheless, for appropriate characterization of TCES materials for meaningful reactor design, the materials need to be characterized in an integrated lab-scale system. Generally, TCES materials are asserted to show better efficiencies in fluidized-bed reactors than fixed and moving-bed reactors. Therefore, experimental and numerical modelling of the system is an essential step in the right direction. Optimizations can be carried out to enhance HAM transfer in the fluidized-bed reactor, for instance, by increasing the contact between the solid and gas. We recommend:

1. Developing novel TCES materials with lower agglomeration tendency, improved thermal conductivity, cyclability, and storage temperatures. This can be achieved by exploring various composites and the addition of suitable nanomaterials;
2. Redesigning fluidized-bed reactors with novel heat exchangers with thermal properties for enabling efficient heat transport over the charge/discharge phases to the HTF;
3. Incorporating a suitable agitator mechanism in the fluidized-bed reactor to facilitate robust particulate interactions, for enhanced HAM transfer coefficients;
4. Finding appropriate simulation models to describe the kinetics of the TCES materials and coupled HAM transfer components of the fluidized-bed reactor. This could be one way to understand all aspects of the integrated thermochemical storage system, and hence maximize the storage potential of this technology.

Author Contributions: Conceptualization, A.K., J.D., J.C., R.B. and M.W.; writing—original draft preparation, A.K.; writing—review and editing, A.K., J.D., J.C., R.B. and M.W.; supervision, J.D.; project administration, J.D.; funding acquisition, J.D. All authors have read and agreed to the published version of the manuscript.

Funding: This research was supported by the Engineering and Physical Sciences Research Council (EPSRC), UK, [grant number EP/V041452/1].

Data Availability Statement: Not applicable.

Acknowledgments: The authors are grateful to the Tertiary Education Trust Fund (tetfund), Nigeria for Anti's studentship award.

Conflicts of Interest: The authors declare no conflict of interest.

References

1. Kumar, M. Social, Economic, and Environmental Impacts of Renewable Energy Resources. *Wind. Sol. Hybrid Renew. Energy Syst.* **2020**, *1*, 89494. [CrossRef]
2. Cooper, S.J.G.; Hammond, G.P. "Decarbonising" UK Industry: Towards a Cleaner Economy. *Proc. Inst. Civ. Eng. Energy* **2018**, *171*, 147–157. [CrossRef]
3. Eames, P.; Loveday, D.; Haines, V.; Romanos, P. The Future Role of Thermal Energy Storage in the UK Energy System. 2014. Available online: <https://ukerc.ac.uk/publications/the-future-role-of-thermal-energy-storage-in-the-uk-energy-system/> (accessed on 4 January 2022).
4. Watson, S.D.; Lomas, K.J.; Buswell, R.A. Decarbonising Domestic Heating: What Is the Peak GB Demand? *Energy Policy* **2019**, *126*, 533–544. [CrossRef]
5. Whittle, B. Decarbonisation of Heat—A Crossroads—Energy Saving Trust. 2019. Available online: <https://energysavingtrust.org.uk/decarbonisation-heat-crossroads/> (accessed on 4 January 2022).
6. Abedin, A.H.; Rosen, M.A. A Critical Review of Thermochemical Energy Storage Systems. *Open Renew. Energy J.* **2011**, *4*, 42–46. [CrossRef]
7. Shilei, L.; Guohui, F.; Neng, Z.; Li, D. Experimental Study and Evaluation of Latent Heat Storage in Phase Change Materials Wallboards. *Energy Build* **2007**, *39*, 1088–1091. [CrossRef]
8. Sunku Prasad, J.; Muthukumar, P.; Desai, F.; Basu, D.N.; Rahman, M.M. A Critical Review of High-Temperature Reversible Thermochemical Energy Storage Systems. *Appl. Energy* **2019**, *254*, 113733. [CrossRef]
9. Chen, X.; Zhang, Z.; Qi, C.; Ling, X.; Peng, H. State of the Art on the High-Temperature Thermochemical Energy Storage Systems. *Energy Convers Manag.* **2018**, *177*, 792–815. [CrossRef]
10. Aydin, D.; Casey, S.P.; Riffat, S. The Latest Advancements on Thermochemical Heat Storage Systems. *Renew. Sustain. Energy Rev.* **2015**, *41*, 356–367. [CrossRef]
11. André, L.; Abanades, S.; Flamant, G. Screening of Thermochemical Systems Based on Solid-Gas Reversible Reactions for High Temperature Solar Thermal Energy Storage. *Renew. Sustain. Energy Rev.* **2016**, *64*, 703–715. [CrossRef]
12. Pardo, P.; Deydier, A.; Anxionnaz-Minvielle, Z.; Rougé, S.; Cabassud, M.; Cognet, P. A Review on High Temperature Thermochemical Heat Energy Storage. *Renew. Sustain. Energy Rev.* **2014**, *32*, 591–610. [CrossRef]
13. Farulla, G.A.; Cellura, M.; Guarino, F.; Ferraro, M. A Review of Thermochemical Energy Storage Systems for Power Grid Support. *Appl. Sci.* **2020**, *10*, 3142. [CrossRef]
14. André, L.; Abanades, S. Recent Advances in Thermochemical Energy Storage via Solid–Gas Reversible Reactions at High Temperature. *Energies* **2020**, *13*, 5859. [CrossRef]
15. Yan, Y.; Wang, K.; Clough, P.T.; Anthony, E.J. Developments in Calcium/Chemical Looping and Metal Oxide Redox Cycles for High-Temperature Thermochemical Energy Storage: A Review. *Fuel Process. Technol.* **2020**, *199*, 106280. [CrossRef]
16. Xu, C.; Yu, Z.; Xie, Y.; Ren, Y.; Ye, F.; Ju, X. Study of the Hydration Behavior of Zeolite-MgSO₄ Composites for Long-Term Heat Storage. *Appl. Therm. Eng.* **2018**, *129*, 250–259. [CrossRef]
17. Scapino, L.; Zondag, H.A.; Van Bael, J.; Diriken, J.; Rindt, C.C.M. Sorption Heat Storage for Long-Term Low-Temperature Applications: A Review on the Advancements at Material and Prototype Scale. *Appl. Energy* **2017**, *190*, 920–948. [CrossRef]
18. Hawwash, A.A.; Hassan, H.; El Feky, K. Impact of Reactor Design on the Thermal Energy Storage of Thermochemical Materials. *Appl. Therm. Eng.* **2020**, *168*, 114776. [CrossRef]
19. Zsembinski, G.; Sole, A.; Barreneche, C.; Prieto, C.; Fernández, A.I.; Cabeza, L.F. Review of Reactors with Potential Use in Thermochemical Energy Storage in Concentrated Solar Power Plants. *Energies* **2018**, *11*, 2358. [CrossRef]
20. Desai, F.; Sunku Prasad, J.; Muthukumar, P.; Rahman, M.M. Thermochemical Energy Storage System for Cooling and Process Heating Applications: A Review. *Energy Convers. Manag.* **2021**, *229*, 113617. [CrossRef]
21. Gbenou, T.R.S.; Fopah-Lele, A.; Wang, K. Recent Status and Prospects on Thermochemical Heat Storage Processes and Applications. *Entropy* **2021**, *23*, 953. [CrossRef]
22. Sadeghi, G. Energy Storage on Demand: Thermal Energy Storage Development, Materials, Design, and Integration Challenges. *Energy Storage Mater.* **2022**, *46*, 192–222. [CrossRef]

23. Marie, L.F.; Landini, S.; Bae, D.; Francia, V.; O'Donovan, T.S. Advances in Thermochemical Energy Storage and Fluidised Beds for Domestic Heat. *J. Energy Storage* **2022**, *53*, 105242. [[CrossRef](#)]
24. Kant, K.; Pitchumani, R. Advances and Opportunities in Thermochemical Heat Storage Systems for Buildings Applications. *Appl. Energy* **2022**, *321*, 119299. [[CrossRef](#)]
25. Salgado-Pizarro, R.; Calderón, A.; Svobodova-Sedlackova, A.; Fernández, A.I.; Barreneche, C. The Relevance of Thermochemical Energy Storage in the Last Two Decades: The Analysis of Research Evolution. *J. Energy Storage* **2022**, *51*, 104377. [[CrossRef](#)]
26. Gbenou, T.R.S.; Fopah-Lele, A.; Wang, K. Macroscopic and Microscopic Investigations of Low-Temperature Thermochemical Heat Storage Reactors: A Review. *Renew. Sustain. Energy Rev.* **2022**, *161*, 112152. [[CrossRef](#)]
27. Ding, Y.; Riffat, S.B. Thermochemical Energy Storage Technologies for Building Applications: A State-of-the-Art Review. *Int. J. Low-Carbon Technol.* **2013**, *8*, 106–116. [[CrossRef](#)]
28. Pan, Z.H.; Zhao, C.Y. Gas–Solid Thermochemical Heat Storage Reactors for High-Temperature Applications. *Energy* **2017**, *130*, 155–173. [[CrossRef](#)]
29. Bauer, T. Fundamentals of High-Temperature Thermal Energy Storage, Transfer, and Conversion. In *Ultra-High Temperature Thermal Energy Storage, Transfer and Conversion*; Elsevier: Amsterdam, The Netherlands, 2021; pp. 1–34.
30. Yu, N.; Wang, R.Z.; Wang, L.W. Sorption Thermal Storage for Solar Energy. *Prog. Energy Combust. Sci.* **2013**, *39*, 489–514. [[CrossRef](#)]
31. Srivastava, N.C.; Eames, I.W. A Review of Adsorbents and Adsorbates in Solid-Vapour Adsorption Heat Pump Systems. *Appl. Therm. Eng.* **1998**, *18*, 707–714. [[CrossRef](#)]
32. Wu, H.; Salles, F.; Zajac, J. A Critical Review of Solid Materials for Low-Temperature Thermochemical Storage of Solar Energy Based on Solid-Vapour Adsorption in View of Space Heating Uses. *Molecules* **2019**, *24*, 945. [[CrossRef](#)]
33. Kuznik, F.; Johannes, K. Thermodynamic Efficiency of Water Vapor/Solid Chemical Sorption Heat Storage for Buildings: Theoretical Limits and Integration Considerations. *Appl. Sci.* **2020**, *10*, 489. [[CrossRef](#)]
34. N'Tsoukpoe, K.E.; Kuznik, F. A Reality Check on Long-Term Thermochemical Heat Storage for Household Applications. *Renew. Sustain. Energy Rev.* **2021**, *139*, 110683. [[CrossRef](#)]
35. Makhanya, N.; Oboirien, B.; Ren, J.; Musyoka, N.; Sciacovelli, A. Recent Advances on Thermal Energy Storage Using Metal-Organic Frameworks (MOFs). *J. Energy Storage* **2021**, *34*, 102179. [[CrossRef](#)]
36. Cabeza, L.F.; Martorell, I.; Miró, L.; Fernández, A.I.; Barreneche, C. Introduction to Thermal Energy Storage (TES) Systems. In *Advances in Thermal Energy Storage Systems: Methods and Applications*; Woodhead Publishing: Sawston, UK, 2015.
37. Carrillo, A.J.; Moya, J.; Bayón, A.; Jana, P.; De La Peña O'Shea, V.A.; Romero, M.; Gonzalez-Aguilar, J.; Serrano, D.P.; Pizarro, P.; Coronado, J.M. Thermochemical Energy Storage at High Temperature via Redox Cycles of Mn and Co Oxides: Pure Oxides versus Mixed Ones. *Sol. Energy Mater. Sol. Cells* **2014**, *123*, 47–57. [[CrossRef](#)]
38. Carrillo, A.J.; González-Aguilar, J.; Romero, M.; Coronado, J.M. Solar Energy on Demand: A Review on High Temperature Thermochemical Heat Storage Systems and Materials. *Chem. Rev.* **2019**, *119*, 4777–4816. [[CrossRef](#)]
39. Felderhoff, M.; Urbanczyk, R.; Peil, S. Thermochemical Heat Storage for High Temperature Applications—A Review. *Green* **2013**, *3*, 113–123. [[CrossRef](#)]
40. Cot-Gores, J.; Castell, A.; Cabeza, L.F. Thermochemical Energy Storage and Conversion: A-State-of-the-Art Review of the Experimental Research under Practical Conditions. *Renew. Sustain. Energy Rev.* **2012**, *16*, 5207–5224. [[CrossRef](#)]
41. Lin, J.; Zhao, Q.; Huang, H.; Mao, H.; Liu, Y.; Xiao, Y. Applications of Low-Temperature Thermochemical Energy Storage Systems for Salt Hydrates Based on Material Classification: A Review. *Sol. Energy* **2021**, *214*, 149–178. [[CrossRef](#)]
42. Clark, R.J.; Mehrabadi, A.; Farid, M. State of the Art on Salt Hydrate Thermochemical Energy Storage Systems for Use in Building Applications. *J. Energy Storage* **2020**, *27*, 101145. [[CrossRef](#)]
43. Marín, P.E.; Milian, Y.; Ushak, S.; Cabeza, L.F.; Grágeda, M.; Shire, G.S.F. Lithium Compounds for Thermochemical Energy Storage: A State-of-the-Art Review and Future Trends. *Renew. Sustain. Energy Rev.* **2021**, *149*, 111381. [[CrossRef](#)]
44. Molenda, M.; Stengler, J.; Linder, M.; Wörner, A. Reversible Hydration Behavior of CaCl₂ at High H₂O Partial Pressures for Thermochemical Energy Storage. *Thermochim. Acta* **2013**, *560*, 76–81. [[CrossRef](#)]
45. Rammelberg, H.U.; Schmidt, T.; Ruck, W. Hydration and Dehydration of Salt Hydrates and Hydroxides for Thermal Energy Storage—Kinetics and Energy Release. *Energy Procedia* **2012**, *30*, 362–369. [[CrossRef](#)]
46. Van Essen, V.M.; Cot Gores, J.; Bleijendaal, L.P.J.; Zondag, H.A.; Schuitema, R.; Bakker, M.; Van Helden, W.G.J. Characterization of Salt Hydrates for Compact Seasonal Thermochemical Storage. In *Proceedings of the ASME 3rd International Conference on Energy Sustainability*, San Francisco, CA, USA, 19–23 July 2009; Volume 2, pp. 825–830.
47. Posern, K.; Kaps, C. Calorimetric Studies of Thermochemical Heat Storage Materials Based on Mixtures of MgSO₄ and MgCl₂. *Thermochim Acta* **2010**, *502*, 73–76. [[CrossRef](#)]
48. Fopah Lele, A.; N'Tsoukpoe, K.E.; Osterland, T.; Kuznik, F.; Ruck, W.K.L. Thermal Conductivity Measurement of Thermochemical Storage Materials. *Appl. Therm. Eng.* **2015**, *89*, 916–926. [[CrossRef](#)]
49. Michel, B.; Neveu, P.; Mazet, N. Comparison of Closed and Open Thermochemical Processes, for Long-Term Thermal Energy Storage Applications. *Energy* **2014**, *72*, 702–716. [[CrossRef](#)]
50. N'Tsoukpoe, K.E.; Le Pierrès, N.; Luo, L. Numerical Dynamic Simulation and Analysis of a Lithium Bromide/Water Long-Term Solar Heat Storage System. *Energy* **2012**, *37*, 346–358. [[CrossRef](#)]

51. Donkers, P.A.J.; Beckert, S.; Pel, L.; Stallmach, F.; Steiger, M.; Adan, O.C.G. Water Transport in $\text{MgSO}_4 \cdot 7\text{H}_2\text{O}$ during Dehydration in View of Thermal Storage. *J. Phys. Chem. C* **2015**, *119*, 28711–28720. [[CrossRef](#)]
52. N'Tsoukpoe, K.E.; Schmidt, T.; Rammelberg, H.U.; Watts, B.A.; Ruck, W.K.L. A Systematic Multi-Step Screening of Numerous Salt Hydrates for Low Temperature Thermochemical Energy Storage. *Appl. Energy* **2014**, *124*, 1–16. [[CrossRef](#)]
53. Donkers, P.A.J.; Pel, L.; Adan, O.C.G. Experimental Studies for the Cyclability of Salt Hydrates for Thermochemical Heat Storage. *J. Energy Storage* **2016**, *5*, 25–32. [[CrossRef](#)]
54. De Jong, A.J.; Trausel, F.; Finck, C.; Van Vliet, L.; Cuypers, R. Thermochemical Heat Storage—System Design Issues. *Energy Procedia* **2014**, *48*, 309–319. [[CrossRef](#)]
55. Gaeini, M.; Shaik, S.A.; Rindt, C.C.M. Characterization of Potassium Carbonate Salt Hydrate for Thermochemical Energy Storage in Buildings. *Energy Build.* **2019**, *196*, 178–193. [[CrossRef](#)]
56. Donkers, P.A.J.; Sögütöglu, L.C.; Huinink, H.P.; Fischer, H.R.; Adan, O.C.G. A Review of Salt Hydrates for Seasonal Heat Storage in Domestic Applications. *Appl. Energy* **2017**, *199*, 45–68. [[CrossRef](#)]
57. Solé, A.; Martorell, I.; Cabeza, L.F. State of the Art on Gas-Solid Thermochemical Energy Storage Systems and Reactors for Building Applications. *Renew. Sustain. Energy Rev.* **2015**, *47*, 386–398. [[CrossRef](#)]
58. Zhao, Y.J.; Wang, R.Z.; Zhang, Y.N.; Yu, N. Development of SrBr₂ Composite Sorbents for a Sorption Thermal Energy Storage System to Store Low-Temperature Heat. *Energy* **2016**, *115*, 129–139. [[CrossRef](#)]
59. Zhao, Q.; Lin, J.; Huang, H.; Wu, Q.; Shen, Y.; Xiao, Y. Optimization of Thermochemical Energy Storage Systems Based on Hydrated Salts: A Review. *Energy Build.* **2021**, *244*, 111035. [[CrossRef](#)]
60. Ait Ousaleh, H.; Sair, S.; Zaki, A.; Faik, A.; Mirena Igartua, J.; El Bouari, A. Double Hydrates Salt as Sustainable Thermochemical Energy Storage Materials: Evaluation of Dehydration Behavior and Structural Phase Transition Reversibility. *Sol. Energy* **2020**, *201*, 846–856. [[CrossRef](#)]
61. D'Entremont, A.; Corgnale, C.; Hardy, B.; Zidan, R. Simulation of High Temperature Thermal Energy Storage System Based on Coupled Metal Hydrides for Solar Driven Steam Power Plants. *Int. J. Hydrogen Energy* **2018**, *43*, 817–830. [[CrossRef](#)]
62. Harries, D.N.; Paskevicius, M.; Sheppard, D.A.; Price, T.E.C.; Buckley, C.E. Concentrating Solar Thermal Heat Storage Using Metal Hydrides. *Proc. IEEE* **2012**, *100*, 539–549. [[CrossRef](#)]
63. Felderhoff, M.; Bogdanović, B. High Temperature Metal Hydrides as Heat Storage Materials for Solar and Related Applications. *Int. J. Mol. Sci.* **2009**, *10*, 325–344. [[CrossRef](#)]
64. Zhang, J.; Sun, L.Q.; Zhou, Y.C.; Peng, P. Dehydrogenation Thermodynamics of Magnesium Hydride Doped with Transition Metals: Experimental and Theoretical Studies. *Comput. Mater. Sci.* **2015**, *98*, 211–219. [[CrossRef](#)]
65. Zhou, C.; Zhang, J.; Bowman, R.C.; Fang, Z.Z. Roles of Ti-Based Catalysts on Magnesium Hydride and Its Hydrogen Storage Properties. *Inorganics* **2021**, *9*, 36. [[CrossRef](#)]
66. Khan, D.; Zou, J.; Zeng, X.; Ding, W. Hydrogen Storage Properties of Nanocrystalline Mg_2Ni Prepared from Compressed 2MgH_2 -Ni Powder. *Int. J. Hydrogen Energy* **2018**, *43*, 22391–22400. [[CrossRef](#)]
67. Banrejee, S.; Kumar, A.; Ruz, P.; Sudarsan, V. Improvement of Hydrogen Storage Characteristics of Catalyst Free Magnesium Nanoparticles Prepared by Wet Milling. *Int. J. Energy Res.* **2021**, *45*, 17597–17608. [[CrossRef](#)]
68. Chen, X.; Zou, J.; Zeng, X.; Ding, W. Hydrogen Storage Properties of a Mg-La-Fe-H Nano-Composite Prepared through Reactive Ball Milling. *J. Alloys Compd.* **2017**, *701*, 208–214. [[CrossRef](#)]
69. Silva, R.A.; Leal Neto, R.M.; Leiva, D.R.; Ishikawa, T.T.; Kiminami, C.S.; Jorge, A.M.; Botta, W.J. Room Temperature Hydrogen Absorption by Mg and Mg-TiFe Nanocomposites Processed by High-Energy Ball Milling. *Int. J. Hydrogen Energy* **2018**, *43*, 12251–12259. [[CrossRef](#)]
70. Kim, K.C. A Review on Design Strategies for Metal Hydrides with Enhanced Reaction Thermodynamics for Hydrogen Storage Applications. *Int. J. Energy Res.* **2018**, *42*, 1455–1468. [[CrossRef](#)]
71. Bogdanovi, B.; Reiser, A.; Schlichte, K.; Spliethoff, B.; Tesche, B. Thermodynamics and Dynamics of the Mg-Fe-H System and Its Potential for Thermochemical Thermal Energy Storage. *J. Alloys Compd.* **2002**, *345*, 77–89. [[CrossRef](#)]
72. Sulaiman, N.N.; Juahir, N.; Mustafa, N.S.; Halim Yap, F.A.; Ismail, M. Improved Hydrogen Storage Properties of MgH_2 Catalyzed with K_2NiF_6 . *J. Energy Chem.* **2016**, *25*, 832–839. [[CrossRef](#)]
73. Abdul Majid, N.A.; Maeda, N.; Notomi, M. Improved Hydrogen Desorption Properties of Magnesium Hydride with $\text{TiFe}_{0.8}\text{Mn}_{0.2}$, Graphite and Iron Addition. *Int. J. Hydrogen Energy* **2019**, *44*, 29189–29195. [[CrossRef](#)]
74. Kumar, E.M.; Rajkamal, A.; Thapa, R. Screening Based Approach and Dehydrogenation Kinetics for MgH_2 : Guide to Find Suitable Dopant Using First-Principles Approach. *Sci. Rep.* **2017**, *7*, 15550. [[CrossRef](#)]
75. Jain, P.; Dixit, V.; Jain, A.; Srivastava, O.N.; Huot, J. Effect of Magnesium Fluoride on Hydrogenation Properties of Magnesium Hydride. *Energies* **2015**, *8*, 12546–12556. [[CrossRef](#)]
76. Zhu, M.; Lu, Y.; Ouyang, L.; Wang, H. Thermodynamic Tuning of Mg-Based Hydrogen Storage Alloys: A Review. *Materials* **2013**, *6*, 4654–4674. [[CrossRef](#)]
77. Darkwa, K. Thermochemical Energy Storage in Inorganic Oxides: An Experimental Evaluation. *Appl. Therm. Eng.* **1998**, *18*, 387–400. [[CrossRef](#)]
78. Schaube, F.; Koch, L.; Wörner, A.; Müller-Steinhagen, H. A Thermodynamic and Kinetic Study of the De- and Rehydration of $\text{Ca}(\text{OH})_2$ at High H_2O Partial Pressures for Thermo-Chemical Heat Storage. *Thermochim. Acta* **2012**, *538*, 9–20. [[CrossRef](#)]

79. Schaube, F.; Kohzer, A.; Schütz, J.; Wörner, A.; Müller-Steinhagen, H. De- and Rehydration of $\text{Ca}(\text{OH})_2$ in a Reactor with Direct Heat Transfer for Thermo-Chemical Heat Storage. Part A: Experimental Results. *Chem. Eng. Res. Des.* **2013**, *91*, 856–864. [[CrossRef](#)]
80. Criado, Y.A.; Alonso, M.; Abanades, J.C. Kinetics of the $\text{CaO}/\text{Ca}(\text{OH})_2$ Hydration/Dehydration Reaction for Thermochemical Energy Storage Applications. *Ind. Eng. Chem. Res.* **2014**, *53*, 12594–12601. [[CrossRef](#)]
81. Dai, L.; Long, X.F.; Lou, B.; Wu, J. Thermal Cycling Stability of Thermochemical Energy Storage System $\text{Ca}(\text{OH})_2/\text{CaO}$. *Appl. Therm. Eng.* **2018**, *133*, 261–268. [[CrossRef](#)]
82. Criado, Y.A.; Alonso, M.; Abanades, J.C. Enhancement of a $\text{CaO}/\text{Ca}(\text{OH})_2$ Based Material for Thermochemical Energy Storage. *Sol. Energy* **2016**, *135*, 800–809. [[CrossRef](#)]
83. Funayama, S.; Takasu, H.; Zamengo, M.; Kariya, J.; Kim, S.T.; Kato, Y. Composite Material for High-temperature Thermochemical Energy Storage Using Calcium Hydroxide and Ceramic Foam. *Energy Storage* **2019**, *1*, e53. [[CrossRef](#)]
84. Funayama, S.; Takasu, H.; Kim, S.T.; Kato, Y. Thermochemical Storage Performance of a Packed Bed of Calcium Hydroxide Composite with a Silicon-Based Ceramic Honeycomb Support. *Energy* **2020**, *201*, 117673. [[CrossRef](#)]
85. Kariya, J.; Ryu, J.; Kato, Y. Reaction Performance of Calcium Hydroxide and Expanded Graphite Composites for Chemical Heat Storage Applications. *ISIJ Int.* **2015**, *55*, 457–463. [[CrossRef](#)]
86. Huang, C.; Xu, M.; Huai, X. Experimental Investigation on Thermodynamic and Kinetic of Calcium Hydroxide Dehydration with Hexagonal Boron Nitride Doping for Thermochemical Energy Storage. *Chem. Eng. Sci.* **2019**, *206*, 518–526. [[CrossRef](#)]
87. Shkatulov, A.; Aristov, Y. Calcium Hydroxide Doped by KNO_3 as a Promising Candidate for Thermochemical Storage of Solar Heat. *RSC Adv.* **2017**, *7*, 42929–42939. [[CrossRef](#)]
88. Wang, T.; Zhao, C.Y.; Yan, J. Investigation on the $\text{Ca}(\text{OH})_2/\text{CaO}$ Thermochemical Energy Storage System with Potassium Nitrate Addition. *Sol. Energy Mater. Sol. Cells* **2020**, *215*, 110646. [[CrossRef](#)]
89. Gollsch, M.; Afflerbach, S.; Angadi, B.; Linder, M. Investigation of Calcium Hydroxide Powder for Thermochemical Storage Modified with Nanostructured Flow Agents. *Sol. Energy* **2020**, *201*, 810–818. [[CrossRef](#)]
90. Cosquillo Mejia, A.; Afflerbach, S.; Linder, M.; Schmidt, M. Experimental Analysis of Encapsulated $\text{CaO}/\text{Ca}(\text{OH})_2$ Granules as Thermochemical Storage in a Novel Moving Bed Reactor. *Appl. Therm. Eng.* **2020**, *169*, 114961. [[CrossRef](#)]
91. Afflerbach, S.; Afflerbach, K.; Trettin, R.; Krumm, W. Improvement of a Semipermeable Shell for Encapsulation of Calcium Hydroxide for Thermochemical Heat Storage Solutions: Material Design and Evaluation in Laboratory and Reactor Scale. *Sol. Energy* **2021**, *217*, 208–222. [[CrossRef](#)]
92. André, L.; Abanades, S. Investigation of Metal Oxides, Mixed Oxides, Perovskites and Alkaline Earth Carbonates/Hydroxides as Suitable Candidate Materials for High-Temperature Thermochemical Energy Storage Using Reversible Solid-Gas Reactions. *Mater Today Energy* **2018**, *10*, 48–61. [[CrossRef](#)]
93. André, L.; Abanades, S. Evaluation and Performances Comparison of Calcium, Strontium and Barium Carbonates during Calcination/Carbonation Reactions for Solar Thermochemical Energy Storage. *J. Energy Storage* **2017**, *13*, 193–205. [[CrossRef](#)]
94. Lu, S.; Wu, S. Calcination-Carbonation Durability of Nano CaCO_3 Doped with Li_2SO_4 . *Chem. Eng. J.* **2016**, *294*, 22–29. [[CrossRef](#)]
95. Daud, F.D.M.; Vignesh, K.; Sreekantan, S.; Mohamed, A.R. Improved CO_2 Adsorption Capacity and Cyclic Stability of CaO Sorbents Incorporated with MgO . *New J. Chem.* **2016**, *40*, 231–237. [[CrossRef](#)]
96. Wang, K.; Gu, F.; Clough, P.T.; Zhao, P.; Anthony, E.J. Porous MgO -Stabilized CaO -Based Powders/Pellets via a Citric Acid-Based Carbon Template for Thermochemical Energy Storage in Concentrated Solar Power Plants. *Chem. Eng. J.* **2020**, *390*, 124163. [[CrossRef](#)]
97. Benitez-Guerrero, M.; Valverde, J.M.; Perejon, A.; Sanchez-Jimenez, P.E.; Perez-Maqueda, L.A. Low-Cost Ca-Based Composites Synthesized by Biotemplate Method for Thermochemical Energy Storage of Concentrated Solar Power. *Appl. Energy* **2018**, *210*, 108–116. [[CrossRef](#)]
98. Chen, X.; Jin, X.; Liu, Z.; Ling, X.; Wang, Y. Experimental Investigation on the CaO/CaCO_3 Thermochemical Energy Storage with SiO_2 Doping. *Energy* **2018**, *155*, 128–138. [[CrossRef](#)]
99. Da, Y.; Xuan, Y.; Teng, L.; Zhang, K.; Liu, X.; Ding, Y. Calcium-Based Composites for Direct Solar-Thermal Conversion and Thermochemical Energy Storage. *Chem. Eng. J.* **2020**, *382*, 122815. [[CrossRef](#)]
100. Sun, H.; Li, Y.; Yan, X.; Zhao, J.; Wang, Z. Thermochemical Energy Storage Performance of $\text{Al}_2\text{O}_3/\text{CeO}_2$ Co-Doped CaO -Based Material under High Carbonation Pressure. *Appl. Energy* **2020**, *263*, 114650. [[CrossRef](#)]
101. Raganati, F.; Chirone, R.; Ammendola, P. Calcium-Looping for Thermochemical Energy Storage in Concentrating Solar Power Applications: Evaluation of the Effect of Acoustic Perturbation on the Fluidized Bed Carbonation. *Chem. Eng. J.* **2020**, *392*, 123658. [[CrossRef](#)]
102. Møller, K.T.; Ibrahim, A.; Buckley, C.E.; Paskevicius, M. Inexpensive Thermochemical Energy Storage Utilising Additive Enhanced Limestone. *J. Mater. Chem. A Mater.* **2020**, *8*, 9646–9653. [[CrossRef](#)]
103. Block, T.; Schmücker, M. Metal Oxides for Thermochemical Energy Storage: A Comparison of Several Metal Oxide Systems. *Sol. Energy* **2016**, *126*, 195–207. [[CrossRef](#)]
104. Silakhori, M.; Jafarian, M.; Arjomandi, M.; Nathan, G.J. Thermogravimetric Analysis of Cu, Mn, Co, and Pb Oxides for Thermochemical Energy Storage. *J. Energy Storage* **2019**, *23*, 138–147. [[CrossRef](#)]
105. Deutsch, M.; Horvath, F.; Knoll, C.; Lager, D.; Gierl-Mayer, C.; Weinberger, P.; Winter, F. High-Temperature Energy Storage: Kinetic Investigations of the $\text{CuO}/\text{Cu}_2\text{O}$ Reaction Cycle. *Energy Fuels* **2017**, *31*, 2324–2334. [[CrossRef](#)]

106. Alonso, E.; Pérez-Rábago, C.; Licurgo, J.; Fuentealba, E.; Estrada, C.A. First Experimental Studies of Solar Redox Reactions of Copper Oxides for Thermochemical Energy Storage. *Sol. Energy* **2015**, *115*, 297–305. [[CrossRef](#)]
107. Gigantino, M.; Brunser, S.S.; Steinfeld, A. High-Temperature Thermochemical Heat Storage via the CuO/Cu₂O Redox Cycle: From Material Synthesis to Packed-Bed Reactor Engineering and Cyclic Operation. *Energy Fuels* **2020**, *34*, 16772–16782. [[CrossRef](#)]
108. André, L.; Abanades, S.; Cassayre, L. Mixed Co, Cu and Mn-Based Metal Oxides for Thermochemical Energy Storage Application. In Proceedings of the AIP Conference Proceedings, Maharashtra, India, 8 November 2018; American Institute of Physics Inc.: College Park, MD, USA, 2018; Volume 2033.
109. Bielsa, D.; Zaki, A.; Faik, A.; Arias, P.L. Efficiency Improvement of Mn₂O₃/Mn₃O₄ Redox Reaction by Means of Different Operation Strategies. In Proceedings of the AIP Conference Proceedings, Bogor, Indonesia, 25 July 2019; American Institute of Physics Inc.: College Park, MD, USA, 2019; Volume 2126.
110. André, L.; Abanades, S.; Cassayre, L. Experimental and Thermodynamic Study of Co-Fe and Mn-Fe Based Mixed Metal Oxides for Thermochemical Energy Storage Application. In Proceedings of the AIP Conference Proceedings, Bydgoszcz, Poland, 27 June 2017; American Institute of Physics Inc.: College Park, MD, USA, 2017; Volume 1850.
111. Neises, M.; Tescari, S.; De Oliveira, L.; Roeb, M.; Sattler, C.; Wong, B. Solar-Heated Rotary Kiln for Thermochemical Energy Storage. *Sol. Energy* **2012**, *86*, 3040–3048. [[CrossRef](#)]
112. Jahromy, S.S.; Birkelbach, F.; Jordan, C.; Huber, C.; Harasek, M.; Werner, A.; Winter, F. Impact of Partial Pressure, Conversion, and Temperature on the Oxidation Reaction Kinetics of Cu₂O to CuO in Thermochemical Energy Storage. *Energies* **2019**, *12*, 508. [[CrossRef](#)]
113. Liu, H.; Wang, W.; Zhang, Y. Performance Gap between Thermochemical Energy Storage Systems Based on Salt Hydrates and Materials. *J. Clean. Prod.* **2021**, *313*, 127908. [[CrossRef](#)]
114. Ferchaud, C.J.; Zondag, H.A.; Veldhuis, J.B.J.; De Boer, R. Study of the Reversible Water Vapour Sorption Process of MgSO₄·7H₂O and MgCl₂·6H₂O under the Conditions of Seasonal Solar Heat Storage. *J. Phys.* **2012**, *395*, 12069.
115. Opel, O.; Rammelberg, H.U.; Gerard, M.; Ruck, W. Thermalchemical Storage Materials Research—TGA/DSC-Hydration Studies. In Proceedings of the International Conference on Sustainable Energy Storage, Belfast, Ireland, 21–24 February 2011.
116. Zondag, H.; Kikkert, B.; Smeding, S.; De Boer, R.; Bakker, M. Prototype Thermochemical Heat Storage with Open Reactor System. *Appl. Energy* **2013**, *109*, 360–365. [[CrossRef](#)]
117. Verga, M.; Armanasco, F.; Guardamagna, C.; Valli, C.; Bianchin, A.; Agresti, F.; Lo Russo, S.; Maddalena, A.; Principi, G. Scaling up Effects of Mg Hydride in a Temperature and Pressure-Controlled Hydrogen Storage Device. *Int. J. Hydrogen Energy* **2009**, *34*, 4602–4610. [[CrossRef](#)]
118. Paskevicius, M.; Sheppard, D.A.; Williamson, K.; Buckley, C.E. Metal Hydride Thermal Heat Storage Prototype for Concentrating Solar Thermal Power. *Energy* **2015**, *88*, 469–477. [[CrossRef](#)]
119. Xia, G.; Tan, Y.; Chen, X.; Sun, D.; Guo, Z.; Liu, H.; Ouyang, L.; Zhu, M.; Yu, X. Monodisperse Magnesium Hydride Nanoparticles Uniformly Self-Assembled on Graphene. *Adv. Mater.* **2015**, *27*, 5981–5988. [[CrossRef](#)]
120. Yan, J.; Zhao, C.Y. Experimental Study of CaO/Ca(OH)₂ in a Fixed-Bed Reactor for Thermochemical Heat Storage. *Appl. Energy* **2016**, *175*, 277–284. [[CrossRef](#)]
121. Yang, Y.; Li, Y.; Yan, X.; Zhao, J.; Zhang, C. Development of Thermochemical Heat Storage Based on CaO/CaCO₃ Cycles: A review. *Energies* **2021**, *14*, 6847. [[CrossRef](#)]
122. Hutchings, K.N.; Wilson, M.; Larsen, P.A.; Cutler, R.A. Kinetic and Thermodynamic Considerations for Oxygen Absorption/Desorption Using Cobalt Oxide. *Solid State Ion* **2006**, *177*, 45–51. [[CrossRef](#)]
123. Agrafiotis, C.; Roeb, M.; Schmücker, M.; Sattler, C. Exploitation of Thermochemical Cycles Based on Solid Oxide Redox Systems for Thermochemical Storage of Solar Heat. Part 1: Testing of Cobalt Oxide-Based Powders. *Sol. Energy* **2014**, *102*, 189–211. [[CrossRef](#)]
124. Mette, B.; Kerskes, H.; Drück, H. Experimental and Numerical Investigations of Different Reactor Concepts for Thermochemical Energy Storage. *Energy Procedia* **2014**, *57*, 2380–2389. [[CrossRef](#)]
125. Foutch, G.L.; Johannes, A.H. Reactors in Process Engineering. In *Encyclopedia of Physical Science and Technology*; Academic Press Inc.: Cambridge, MA, USA, 2003.
126. Schmidt, M.; Szczukowski, C.; Roßkopf, C.; Linder, M.; Wörner, A. Experimental Results of a 10 KW High Temperature Thermochemical Storage Reactor Based on Calcium Hydroxide. *Appl. Therm. Eng.* **2014**, *62*, 553–559. [[CrossRef](#)]
127. Ranjha, Q.A.; Vahedi, N.; Oztekin, A. Numerical Study of Thermochemical Storage Using Ca(OH)₂/CaO—High Temperature Applications. In Proceedings of the ASME International Mechanical Engineering Congress and Exposition, Proceedings (IMECE), Phoenix, AZ, USA, 11–17 November 2016; Volume 6B-2016.
128. Funayama, S.; Takasu, H.; Zamengo, M.; Kariya, J.; Kim, S.T.; Kato, Y. Performance of Thermochemical Energy Storage of a Packed Bed of Calcium Hydroxide Pellets. *Energy Storage* **2019**, *1*, e40. [[CrossRef](#)]
129. Schmidt, M.; Linder, M. A Novel Thermochemical Long Term Storage Concept: Balance of Renewable Electricity and Heat Demand in Buildings. *Front. Energy Res.* **2020**, *8*, 00137. [[CrossRef](#)]
130. Schmidt, M.; Gutierrez, A.; Linder, M. Thermochemical Energy Storage with CaO/Ca(OH)₂—Experimental Investigation of the Thermal Capability at Low Vapor Pressures in a Lab Scale Reactor. *Appl. Energy* **2017**, *188*, 672–681. [[CrossRef](#)]
131. Peng, X.; Yao, M.; Root, T.W.; Maravelias, C.T. Design and Analysis of Concentrating Solar Power Plants with Fixed-Bed Reactors for Thermochemical Energy Storage. *Appl. Energy* **2020**, *262*, 114543. [[CrossRef](#)]

132. Schaube, F.; Utz, I.; Wörner, A.; Müller-Steinhagen, H. De- and Rehydration of $\text{Ca}(\text{OH})_2$ in a Reactor with Direct Heat Transfer for Thermo-Chemical Heat Storage. Part B: Validation of Model. *Chem. Eng. Res. Des.* **2013**, *91*, 865–873. [[CrossRef](#)]
133. Schmidt, M.; Gollsch, M.; Giger, F.; Grün, M.; Linder, M. Development of a Moving Bed Pilot Plant for Thermochemical Energy Storage with $\text{CaO}/\text{Ca}(\text{OH})_2$. *AIP Conf. Proc.* **2016**, *1734*, 050041.
134. Shirzad, M.; Karimi, M.; Silva, J.A.C.; Rodrigues, A.E. Moving Bed Reactors: Challenges and Progress of Experimental and Theoretical Studies in a Century of Research. *Ind. Eng. Chem. Res.* **2019**, *58*, 9179–9198. [[CrossRef](#)]
135. Angerer, M.; Becker, M.; Härzschel, S.; Kröper, K.; Gleis, S.; Vandersickel, A.; Spliethoff, H. Design of a MW-Scale Thermo-Chemical Energy Storage Reactor. *Energy Rep.* **2018**, *4*, 507–519. [[CrossRef](#)]
136. Preisner, N.C.; Bürger, I.; Wokon, M.; Linder, M. Numerical Investigations of a Counter-Current Moving Bed Reactor for Thermochemical Energy Storage at High Temperatures. *Energies* **2020**, *13*, 772. [[CrossRef](#)]
137. Preisner, N.C.; Linder, M. A Moving Bed Reactor for Thermochemical Energy Storage Based on Metal Oxides. *Energies* **2020**, *13*, 1232. [[CrossRef](#)]
138. Huang, W.; Korba, D.; Randhir, K.; Petrasch, J.; Klausner, J.; AuYeung, N.; Li, L. Thermochemical Reduction Modeling in a High-Temperature Moving-Bed Reactor for Energy Storage: 1D Model. *Appl. Energy* **2022**, *306*, 118009. [[CrossRef](#)]
139. Di Renzo, A.; Scala, F.; Heinrich, S. Recent Advances in Fluidized Bed Hydrodynamics and Transport Phenomena—Progress and Understanding. *Processes* **2021**, *9*, 639. [[CrossRef](#)]
140. Zondag, H.A.; Van Essen, V.M.; Bakker, M. Application of $\text{MgCl}_2 \cdot 6\text{H}_2\text{O}$ for Thermochemical Seasonal Solar Heat Storage. In Proceedings of the 5th International Renewable Energy Storage Conference IRES 2010, Berlin, Germany, 22–24 November 2010.
141. Delhomme, B.; De Rango, P.; Marty, P.; Bacia, M.; Zawilski, B.; Raufast, C.; Miraglia, S.; Fruchart, D. Large Scale Magnesium Hydride Tank Coupled with an External Heat Source. *Int. J. Hydrogen Energy* **2012**, *37*, 9103–9111. [[CrossRef](#)]
142. Meier, A.; Bonaldi, E.; Cella, G.M.; Lipinski, W.; Wuillemain, D.; Palumbo, R. Design and Experimental Investigation of a Horizontal Rotary Reactor for the Solar Thermal Production of Lime. *Energy* **2004**, *29*, 811–821. [[CrossRef](#)]
143. Meroueh, L.; Yenduru, K.; Dasgupta, A.; Jiang, D.; AuYeung, N. Energy Storage Based on SrCO_3 and Sorbents—A Probabilistic Analysis towards Realizing Solar Thermochemical Power Plants. *Renew. Energy* **2019**, *133*, 770–786. [[CrossRef](#)]
144. Flegkas, S.; Birkelbach, F.; Winter, F.; Groenewold, H.; Werner, A. Profitability Analysis and Capital Cost Estimation of a Thermochemical Energy Storage System Utilizing Fluidized Bed Reactors and the Reaction System $\text{MgO}/\text{Mg}(\text{OH})_2$. *Energies* **2019**, *12*, 4788. [[CrossRef](#)]
145. Flegkas, S.; Birkelbach, F.; Winter, F.; Freiburger, N.; Werner, A. Fluidized Bed Reactors for Solid-Gas Thermochemical Energy Storage Concepts—Modelling and Process Limitations. *Energy* **2018**, *143*, 615–623. [[CrossRef](#)]
146. Rougé, S.; Criado, Y.A.; Soriano, O.; Abanades, J.C. Continuous $\text{CaO}/\text{Ca}(\text{OH})_2$ Fluidized Bed Reactor for Energy Storage: First Experimental Results and Reactor Model Validation. *Ind. Eng. Chem. Res.* **2017**, *56*, 844–852. [[CrossRef](#)]
147. Mu, L.; Buist, K.A.; Kuipers, J.A.M.; Deen, N.G. Hydrodynamic and Heat Transfer Study of a Fluidized Bed by Discrete Particle Simulations. *Process.* **2020**, *8*, 463. [[CrossRef](#)]
148. Darkwa, K.; Ianakiev, A.; O’Callaghan, P.W. Modelling and Simulation of Adsorption Process in a Fluidised Bed Thermochemical Energy Reactor. *Appl. Therm. Eng.* **2006**, *26*, 838–845. [[CrossRef](#)]
149. Kim, J.; Han, G.Y. Effect of Agitation on Fluidization Characteristics of Fine Particles in a Fluidized Bed. *Powder Technol.* **2006**, *166*, 113–122. [[CrossRef](#)]
150. Wang, J.J.; Han, Y.; Gu, X.P.; Feng, L.F.; Hu, G.H. Effect of Agitation on the Fluidization Behavior of a Gas-Solid Fluidized Bed with a Frame Impeller. *AIChE J.* **2013**, *59*, 1066–1074. [[CrossRef](#)]
151. Lv, B.; Deng, X.; Shi, C.; Fang, C. Effect of Agitation on Hydrodynamics and Separation Performance of Gas-Solid Separation Fluidized Bed. *Powder Technol.* **2021**, *388*, 129–138. [[CrossRef](#)]
152. Dong, K.; Zhou, Y.; Huang, Z.; Wang, J.; Yang, Y. Gas Bubble Behaviors in a Gas-Solid Fluidized Bed with an Arch Agitator. *Powder Technol.* **2014**, *266*, 38–44. [[CrossRef](#)]
153. Shi, D.P.; Luo, Z.H.; Guo, A.Y. Numerical Simulation of the Gas-Solid Flow in Fluidized-Bed Polymerization Reactors. *Ind. Eng. Chem. Res.* **2010**, *49*, 4070–4079. [[CrossRef](#)]
154. Tafrishi, H.; Sadeghzadeh, S.; Ahmadi, R. Molecular Dynamics Simulations of Phase Change Materials for Thermal Energy Storage: A Review. *RSC Adv.* **2022**, *12*, 14776–14807. [[CrossRef](#)] [[PubMed](#)]
155. Shkatulov, A.; Becit, B.; Zahn, D. Molecular Dynamics Simulations of Nitrate/MgO Interfaces and Understanding Metastability of Thermochemical Materials. *ACS Omega* **2022**, *7*, 16371–16379. [[CrossRef](#)] [[PubMed](#)]
156. Xu, M.; Huai, X.; Cai, J. Agglomeration Behavior of Calcium Hydroxide/Calcium Oxide as Thermochemical Heat Storage Material: A Reactive Molecular Dynamics Study. *J. Phys. Chem. C* **2017**, *121*, 3025–3033. [[CrossRef](#)]
157. Alvares, C.M.S.; Deffrennes, G.; Pisch, A.; Jakse, N. Thermodynamics and Structural Properties of CaO : A Molecular Dynamics Simulation Study. *J. Chem. Phys.* **2020**, *152*, 084503. [[CrossRef](#)]
158. Wang, S.; Shen, Y. Coarse-Grained CFD-DEM Modelling of Dense Gas-Solid Reacting Flow. *Int. J. Heat Mass Transf.* **2022**, *184*, 122302. [[CrossRef](#)]
159. Shen, J.; Liu, X.; Ho, W.H. CFD Simulation of a Fluidized Bed as a Solar Receiver. In Proceedings of the AIP Conference Proceedings, College Park, MD, USA, 25 July 2019; American Institute of Physics Inc.: College Park, MD, USA, 2019; Volume 2126.
160. Bowen, Y.; Jun, Y.; Changying, Z. Investigating the Performance of a Fluidized Bed Reactor for a Magnesium Hydroxide Thermochemical Energy Storage System. *Energy Storage Sci. Technol.* **2021**, *10*, 1735–1744. [[CrossRef](#)]

161. Li, Z.; Xu, M.; Huai, X.; Huang, C.; Wang, K. Simulation and Analysis of Thermochemical Seasonal Solar Energy Storage for District Heating Applications in China. *Int. J. Energy Res.* **2021**, *45*, 7093–7107. [[CrossRef](#)]
162. Ghosh, S.; Fennell, P.S. Design and Techno-Economic Analysis of a Fluidized Bed-Based CaO/Ca(OH)₂ Thermochemical Energy Combined Storage/Discharge Plant with Concentrated Solar Power. In Proceedings of the AIP Conference Proceedings, Daegu, Republic of Korea, 1–4 October 2019; American Institute of Physics Inc.: College Park, MD, USA, 2020; Volume 2303.
163. Alobaid, F.; Almohammed, N.; Massoudi Farid, M.; May, J.; Rößger, P.; Richter, A.; Epple, B. Progress in CFD Simulations of Fluidized Beds for Chemical and Energy Process Engineering. *Prog. Energy Combust. Sci.* **2021**, *19*, 100930.

Disclaimer/Publisher's Note: The statements, opinions and data contained in all publications are solely those of the individual author(s) and contributor(s) and not of MDPI and/or the editor(s). MDPI and/or the editor(s) disclaim responsibility for any injury to people or property resulting from any ideas, methods, instructions or products referred to in the content.